ANNUAL REVIEWS

Annual Review of Marine Science

Turbulence and Coral Reefs

Kristen A. Davis,[1] Geno Pawlak,[2] and Stephen G. Monismith[3]

[1]Department of Civil and Environmental Engineering and Department of Earth System Science, University of California, Irvine, California 92697, USA; email: davis@uci.edu

[2]Department of Mechanical and Aerospace Engineering, University of California, San Diego, La Jolla, California 92093, USA

[3]Department of Civil and Environmental Engineering, Stanford University, Stanford, California 94305, USA

Annu. Rev. Mar. Sci. 2021. 13:343–73

First published as a Review in Advance on August 7, 2020

The *Annual Review of Marine Science* is online at marine.annualreviews.org

https://doi.org/10.1146/annurev-marine-042120-071823

Keywords

turbulence, coral reefs, rough boundary layers, mass transfer, canopy flow, waves

Abstract

The interaction of coral reefs, both chemically and physically, with the surrounding seawater is governed, at the smallest scales, by turbulence. Here, we review recent progress in understanding turbulence in the unique setting of coral reefs—how it influences flow and the exchange of mass and momentum both above and within the complex geometry of coral reef canopies. Flow above reefs diverges from canonical rough boundary layers due to their large and highly heterogeneous roughness and the influence of surface waves. Within coral canopies, turbulence is dominated by large coherent structures that transport momentum both into and away from the canopy, but it is also generated at smaller scales as flow is forced to move around branches or blades, creating wakes. Future work interpreting reef-related observations or numerical models should carefully consider the influence that spatial variation has on momentum and scalar flux.

1. INTRODUCTION

Coral reefs are among the most diverse ecosystems on the planet (Veron 1995). They play an important role protecting coastlines from the damaging effects of waves, provide nurseries for many ocean fish species, and represent a vital source of food for developing nations (Burke et al. 2011, Ferrario et al. 2014). Additionally, reefs are biogeochemical reactors, where the high metabolism of the benthic community transforms and recycles carbon, nitrogen, and other nutrients for marine food chains (D'elia & Wiebe 1990). The interaction of coral reefs, both chemically and physically, with the surrounding seawater is governed by flow—at the large scales by tides, mesoscale currents, and waves and at the smallest scales by turbulence.

Oceanic forcing shapes regional circulation patterns and the horizontal transport of water masses with different properties to the reef, governing the environmental conditions and the dispersal of reef larvae and, thus, the biogeographical distribution of reef organisms (reviewed in Lowe & Falter 2015). However, turbulent mixing governs the vertical coupling between the bed and the overlying water, determining the vertical transport of heat, food, pollutants, pathogens, larvae, and nutrients to or from the benthic reef community (Thomas & Atkinson 1997; Sebens et al. 1998, 2003; Falter et al. 2004, 2007; Reidenbach et al. 2009; Monismith et al. 2010). A review of reef-scale hydrodynamics and boundary layer flows over reefs has been published by Monismith (2007). Here, we focus on the smallest scales of water motion on coral reefs—turbulence.

This review is motivated, in part, by a defining physical characteristic of coral reefs that makes them a good place to study turbulence—their extreme hydrodynamic roughness. While natural surfaces under the erosive influence of breaking waves and strong currents would tend to be worn smooth, scleractinian (hard) corals actively grow complex structures ("roughness elements" to fluid dynamicists) that induce mixing and enhance turbulent fluxes near the bed (e.g., van Woesik et al. 2012). The geometric complexity of corals can be seen from the scale of individual coral colonies, with their various morphologies (e.g., branching, foliated, massive, and encrusting forms), to the scale of reef platforms, where steeply sloping forereefs cut with spur-and-groove formations differ greatly from the wide, shallow reef flats and bommie-filled lagoons in **Figure 1**. Spatially variable reef structure creates correspondingly complex hydrodynamic regimes that are shaped, in part, by the height of the coral reef canopy, h_c, relative to the depth of the water column, h, and the

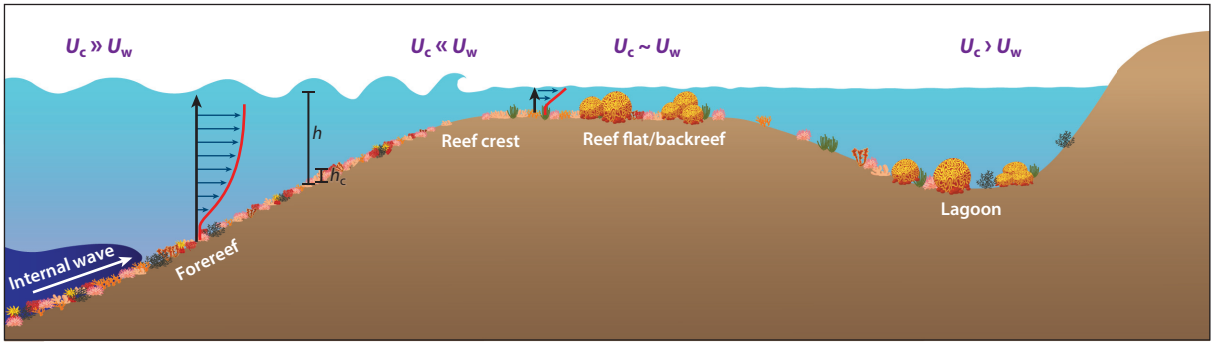

Figure 1

Schematic of a coral reef system with some common biogeographic zones: the deep forereef, where mean flows are often oriented alongshore; the shallow forereef/reef crest, which is heavily influenced by the energetic dissipation of wave energy; the reef flat/backreef zone, where flow is driven by wave setup offshore and tidal flows and coral canopies can fill the entire water column; and deeper lagoons, where flow is fairly tranquil and sheltered from waves. Each zone of the reef is characterized by relative magnitudes of steady (U_c) to oscillatory, wave-driven (U_w) flow velocities and by the scale of the roughness (h_c) relative to the overall flow depth (h).

strength of wave-driven flows, U_w, relative to mean unidirectional currents, U_c (**Figure 2**; for a summary of variables used in this review, see **Table 1**).

Structural complexity creates manifold microhabitats and is thought to be a key feature influencing ecological processes on reefs—affecting the availability of food and the abundance of fish, enhancing herbivory by reef fishes to reduce algae cover, and providing shelter from predators (Holbrook et al. 2002, Gratwicke & Speight 2005, Harborne et al. 2012, Graham & Nash 2013). The interdisciplinary nature of science on coral reefs has led to various methods for defining and quantifying the structural complexity of the benthic community. One of the most common methods of quantifying bottom roughness in marine ecological studies is the chain-and-tape estimate of rugosity, which is the ratio of the contour length along the substrate surface to the corresponding projected horizontal length (Risk 1972). Recent efforts to quantify the complex, multiscale benthic topography of coral reefs have found success in fractal theory (Zawada & Brock 2009, Duvall et al. 2019). Hydrodynamic studies quantify roughness as standard deviation (Lowe et al. 2005a), root-mean-square (rms) slope (Rogers et al. 2018), or roughness density, the total frontal area of canopy elements per horizontal area (Schlichting 1937, Dvorak 1969, Wooding et al. 1973, Jiménez 2004). Most often, however, physical oceanographers are interested in how the roughness elements of the benthic reef community impose large bottom stresses on the flow, characterizing this effect through drag coefficients (C_D), hydrodynamic roughness (z_0), and friction factors (f_w and f_e) (Lowe et al. 2005a, Monismith 2007). For example, estimated drag coefficients over coral reef communities are commonly one to two orders of magnitude higher than those for sandy or muddy coastal beds (Heathershaw & Simpson 1978, Lugo-Fernandez et al. 1998, Lentz et al. 2017).

This review focuses on recent progress in understanding turbulence in the unique setting of coral reefs. We develop a mathematical framework for our discussion in Section 2. We draw insights from relevant engineering literature on flow over rough surfaces and studies of atmospheric flow over vegetation and urban canopies in Section 3. The shallow setting of many reef environments requires consideration of the influence of the free surface and waves on turbulent flows (Section 4). For reefs exposed to internal waves, stratified turbulent boundary layer dynamics become relevant (Section 5). We consider turbulent flow within coral canopies (Section 6), as it is important for mass transport (Section 7), predation of corals by fish, particle capture by corals, and larval settlement.

2. THE ANALYSIS FRAMEWORK

Here, we present the equations governing flow in and above coral canopies and define some useful terms and notations that will be used throughout the article. We adopt right-handed Cartesian coordinates, where $\mathbf{x} = [x,y,z]$ represents the three-dimensional spatial coordinate axes and $\mathbf{u} = [u,v,w]$ is the corresponding velocity vector. For the simplest case of unidirectional flow, turbulent quantities can be represented using a Reynolds decomposition of the velocity vector and other scalar quantities, shown here for the u component of velocity as

$$u = \bar{u} + u', \qquad 1.$$

where the overbar represents a time average and the prime denotes a fluctuating, or turbulent, quantity. Using this notation within the equation for conservation of momentum and taking the time average results in the Reynolds-averaged Navier–Stokes equation, here presented in two dimensions—x, streamwise horizontal and parallel to the bed, and z, normal to the bed ($z = 0$ at the bed):

$$\frac{D\bar{u}}{Dt} = -\frac{1}{\rho}\frac{\partial \bar{p}}{\partial x} + \frac{1}{\rho}\frac{\partial \tau_{xz}}{\partial z}, \qquad 2.$$

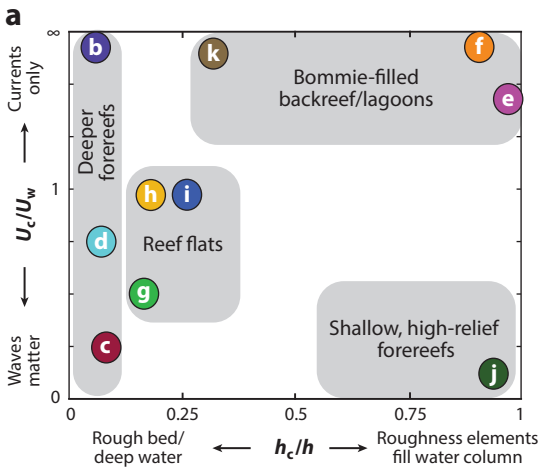

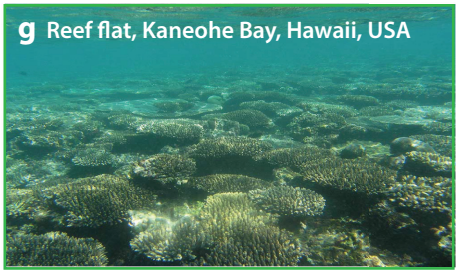

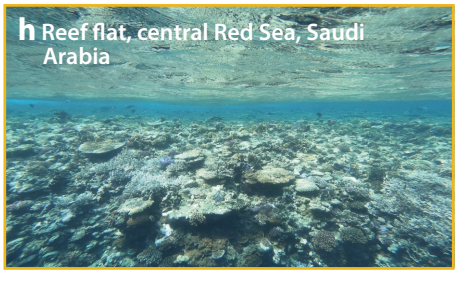

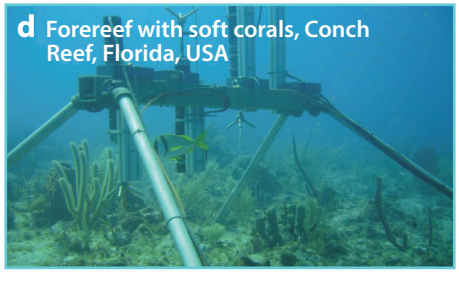

(*Caption appears on following page*)

Figure 2 (*Figure appears on preceding page*)

(*a*) Coral reef environments classified by flow environment and roughness ratio for the studied reef locations pictured in (*b*) Eilat, Israel (Reidenbach et al. 2006); (*c*) Dongsha Atoll, Taiwan, South China Sea (Reid et al. 2019, Davis et al. 2020); (*d*) Conch Reef, Florida, USA (Davis & Monismith 2011); (*e*) Ofu, American Samoa (Green 2002, Rogers et al. 2018); (*f*) Moorea, French Polynesia (Hench & Rosman 2013); (*g*) Kaneohe Bay, Hawaii, USA (Lowe et al. 2005a); (*h*) the central Red Sea, Saudi Arabia (Lentz et al. 2016, 2017); and (*i*) Ningaloo Reef, Australia (Taebi et al. 2011, Pomeroy et al. 2012), along with two locations not pictured: (*j*) Ipam, Guam (Péquignet et al. 2011), and (*k*) Lady Elliot Island, Australia (Huang et al. 2012).

where t is time, p is pressure, ρ is the fluid density, and τ_{xz} is defined here as a sum of the Reynolds stress and the viscous stress,

$$\tau_{xz} = -\rho\overline{u'w'} + \mu\frac{\partial\bar{u}}{\partial z}, \qquad 3.$$

and where μ is fluid viscosity. Equation 2 is relevant for unidirectional flow above canopies, but surface gravity waves are a common feature of coral reef habitats. Oscillatory wave-driven flow can significantly enhance turbulence in a region near the bed called the wave boundary layer (Grant & Madsen 1986, Trowbridge & Lentz 2018). Turbulent motions in the presence of waves complicate the usual Reynolds decomposition for velocity, with the introduction of wave-correlated motions:

$$u = \bar{u} + \tilde{u} + u', \qquad 4.$$

where the second term, $\tilde{u}$, added relative to Equation 1, represents motions that are coherent with the wave phase.

The time-averaged vertical stress in the presence of waves includes an extra stress (relative to Equation 3) that is due to the temporal correlation of oscillatory velocities:

$$\tau_{xz} = -\rho\overline{u'w'} - \rho\overline{\tilde{u}\tilde{w}} + \mu\frac{\partial\bar{u}}{\partial z}. \qquad 5.$$

For high Reynolds numbers, which are typical of reef environments, the last term in Equations 3 and 5 is generally negligible. Other stress terms (τ_{xx}, τ_{yy}, and τ_{xy}), not included here, will also be relevant in flow regions with significant horizontal variability or in the presence of waves, including radiation stress terms (Longuet-Higgins & Stewart 1964).

Within the canopy, the effect of the roughness elements is felt more directly, as flow must move around coral branches, heads, blades of macroalgae, and other canopy elements, creating a highly variable spatial flow structure that is challenging to characterize, even for the simplest geometric approximations of canopy elements (Lowe et al. 2005b). To represent the effect of this complex instantaneous flow field on the mean velocities within the canopy, it is common to employ a double-averaging method with the Reynolds-averaged Navier–Stokes equations—both in time, as is commonly done, and in space over a horizontal plane to remove element-scale spatial heterogeneity (Raupach & Shaw 1982). Using this idea, one can further break down time-averaged quantities as

$$\bar{u} = \langle\bar{u}\rangle + u'', \qquad 6.$$

where the angled brackets denote a spatial average over a horizontal plane (excluding the solid parts of the canopy elements) and double primes denote deviations from the spatial mean. The double-averaged, two-dimensional momentum equation for unidirectional flow within a canopy becomes

$$\frac{\mathrm{D}\langle\bar{u}\rangle}{\mathrm{D}t} = -\frac{1}{\rho}\frac{\partial\langle\bar{p}\rangle}{\partial x} + \frac{1}{\rho}\frac{\partial\langle\tau_{xz}\rangle}{\partial z} - F_x, \qquad 7.$$

Table 1 Summary of variables used in this review

Variable	Unit	Description
A	m	Wave orbital amplitude
A_T	m^2	Total plan area of bed
b	m	Characteristic lateral roughness spacing
C	kg m^{-3}	Concentration of a scalar
C_D	—	Coefficient of drag
C_d	—	Coefficient of drag associated with canopy structure
D	N	Drag force
F	kg m^{-2} s^{-1}	Flux of a scalar
F_x	m s^{-2}	Spatially averaged drag force per volume exerted by the canopy on the flow
f_e	—	Wave energy dissipation factor
f_w	—	Wave friction factor
h	m	Water depth
h_c	m	Canopy height
K_t	m^2 s^{-1}	Turbulent diffusivity of a scalar
k	m	Characteristic physical roughness length scale
k_s	m	Characteristic/equivalent sand grain roughness
L_c	m	Characteristic horizontal scale for heterogeneity
P	—	Roughness parameter
p	N m^{-2}	Pressure
s	m	Characteristic lateral roughness length scale
T	s	Wave period
t	s	Time
U	m s^{-1}	Characteristic flow velocity
U_c	m s^{-1}	Characteristic steady, unidirectional flow velocity
U_w	m s^{-1}	Characteristic oscillatory flow velocity
U_{δ_b}	m s^{-1}	Velocity at the blending height
$\mathbf{u} = [u,v,w]$	m s^{-1}	Flow velocity in three-dimensional space; $\mathbf{x} = [x,y,z]$
u_*	m s^{-1}	Friction or shear velocity
V_t	m s^{-1}	Mass transfer velocity
w	m	Characteristic roughness spacing
z_0	m	Hydrodynamic roughness
z_{ref}	m	Hydrodynamic origin or displacement height
δ	m	Boundary layer thickness
δ_b	m	Blending height
ε_f	m^2 s^{-3}	Dissipation of wave energy due to bed friction
ζ_0	m	Hydrodynamic origin (relative to top of roughness)
λ	—	Roughness density, frontal area of elements per plan area
μ	kg m^{-1} s^{-1}	Fluid viscosity
ν	m^2 s^{-1}	Kinematic viscosity
ν_t	m^2 s^{-1}	Turbulent diffusivity of momentum
ρ	kg m^{-3}	Fluid density
τ_{xz}	kg m^{-1} s^{-2}	Shear stress
τ_b	kg m^{-1} s^{-2}	Shear stress at the bed
ϕ_{wc}	rad	Angle between waves and steady current
ω	s^{-1}	Vorticity

where

$$\langle \tau_{xz} \rangle = -\rho \left\langle \overline{u'w'} \right\rangle - \rho \left\langle \bar{u}''\bar{w}'' \right\rangle + \mu \frac{\partial \langle \bar{u} \rangle}{\partial z} \qquad 8.$$

is the spatially averaged total stress, in which an extra term, $\langle \bar{u}''\bar{w}'' \rangle$, called the dispersive stress, appears, accounting for the spatial correlations in the time-averaged velocity field. Inside coral canopies, spatially variable geometry can generate persistent spatial gradients in flow, making the dispersive stress of similar importance to the Reynolds stress (Asher & Shavit 2019). The last term in Equation 7, F_x, represents the spatially averaged drag force exerted by the canopy elements onto the surrounding flow.

3. TURBULENCE AND MIXING OVER ROUGH TERRAIN

Turbulence in coral reef environments arises through a variety of mechanisms, including breaking surface waves, breaking internal waves, boundary layers over coral elements, and free shear layers from separated flows around those elements. The latter two mechanisms are distinctive to coral reefs relative to other environmental settings due to the extreme, complex nature of coral surfaces. Flows over terrestrial vegetated canopies (e.g., Belcher et al. 2012) are most similar, though the ubiquity of oscillatory motion due to surface waves sets coral reefs further apart.

The key quantity that characterizes the turbulence and overall structure for unstratified flow interaction with a boundary is the net rate of loss of fluid momentum or, equivalently, the drag force that the boundary exerts on the fluid. Total bottom stress, τ_b, is generally given in terms of force per unit area and is manifested at the boundary via viscous shear stress and pressure drag on roughness elements. For rough boundaries at high Reynolds numbers, the latter is dominant (Jiménez 2004). The total stress is also given in terms of a friction velocity $u_* = \sqrt{\tau_b/\rho}$, where ρ is water density. The drag (D) on the flow (per unit area, A_T) is given, using a quadratic drag law, as

$$\tau_b = \frac{D}{A_T} = \rho C_D U^2, \qquad 9.$$

where U is a suitably defined reference velocity, often chosen based on a reference height or using a depth average. This choice, of course, can result in differing values for the drag coefficient, C_D, and potentially complicates comparisons between reported measurements (Rosman & Hench 2011).

Starting with canonical considerations of unstratified steady and oscillatory flow interaction with a rough boundary (see Grant & Madsen 1986, Trowbridge & Lentz 2018), we can identify a suite of relevant dimensionless parameters that will describe the interaction of flow with reef roughness and subsequent turbulent flow characteristics in terms of the friction velocity:

$$u_* = u_* \left(U_c/U_w, \phi_{wc}, k/h, k/A, P\right). \qquad 10.$$

The first parameter represents the relative magnitude of steady (U_c) to oscillatory (U_w) velocities. The second parameter, ϕ_{wc}, is the relative angle between waves and steady flow. The third and fourth parameters relate a characteristic physical roughness length scale of the bed, k, to the total water depth, h, and to the wave orbital amplitude, $A = U_w T$, respectively. Thus, obtaining some parametric representation of the influence of the reef surface geometry on the flow is a key issue. Reef surfaces are inherently multiscaled, so that the choice for the characteristic scale, k, and its connection to the hydrodynamics is not immediately clear. The last parameter, P, then represents some measure (or set of measures) that captures the effects of the complex distribution of roughness scales on the flow. As discussed further below, these measures can include spectral distributions, solidity, and roughness density, among others.

Because relevant velocity and roughness scales are large, reefs are assumed to be fully rough and turbulent, so the Reynolds number is not typically considered a distinctive parameter. Near coral surfaces, at the scale of individual coral communities and within canopies, viscous effects will likely play important roles.

3.1. Canonical Rough Boundary Layer

In the classic paradigm for flow over a homogeneously rough boundary, at some distance above the bed, the flow velocity depends only on u_*; some characteristic length scale for the roughness, z_0; and the distance from the boundary, z. Dimensional considerations then require that the time-averaged velocity $U(z)$ follow a logarithmic profile:

$$\frac{U(z)}{u_*} = \frac{1}{\kappa} \ln \frac{z}{z_0} \qquad 11.$$

(Pope 2000), where $\kappa \sim 0.4$ is the von Kármán constant (Long et al. 1993, Bailey et al. 2014). Equation 11, an expression of the so-called law of the wall, applies where the distance from the wall is much greater than the roughness scale, $z \gg z_0$, and much smaller than the overall boundary layer thickness, δ. The length scale z_0 in the log profile is more accurately the hydrodynamic roughness and represents the height at which the average velocity would vanish if extrapolated downward. This quantity is typically determined from empirical fits of Equation 11 to measured velocity profiles. In actuality, the velocity near $z \sim z_0$ is modified by details of the roughness and, especially for coral reefs, by the turbulent wave boundary layer. The relation between the hydrodynamic roughness length and a representative physical roughness scale k introduced in Equation 10 is not explicit, however. A relation for sand grain roughness, obtained by Nikuradse (1933), is commonly used for homogeneous roughness: $z_0 = k_s/30$, where k_s is a characteristic sand grain size. For more complex roughness characterized by multiple length scales, the transfer function is not so clear, as discussed further below.

Large and highly variable roughness for coral reef surfaces complicates the definition of the vertical coordinate in Equation 11. An arbitrarily defined vertical coordinate z' can be related to the coordinate z in Equation 11, introducing the hydrodynamic origin or displacement height, $z_{\text{ref}} = z - z'$ (Raupach et al. 1991). Jackson (1981) showed that this location corresponds to the height at which the hydrodynamic drag force is applied to the surface. For widely spaced, regular transverse square bars, Leonardi et al. (2003) showed that this height was at roughly half of the element height.

The parameters in Equation 11 are defined differently across various fields of application. For example, in engineering literature, the velocity offset associated with z_0 is commonly given as a roughness function ΔU^+, and Equation 11 is expressed in nondimensional form as

$$U^+ = \frac{1}{\kappa} \ln z^+ - \Delta U^+. \qquad 12.$$

Here, the superscript plus refers to nondimensional values scaled using a viscous length ν/u_*, so that $U^+ = U(z)/u_*$ and $z^+ = zu_*/\nu$. The roughness function is then related to the reduction in the velocity profile for the rough boundary case relative to that for a smooth wall (Jiménez 2004).

Equations 11 and 12 apply within a limited region near the boundary where the overall boundary layer thickness is not yet relevant. For open-channel flows where the boundary layer is fully developed, so that the boundary effects extend throughout the water column, Equations 11 and 12 can accurately describe velocity profiles for $z < 0.2h$ (Nezu & Nakagawa 1993). Outside of this region, the deviation of the mean velocity from the log profile can be accounted for by addition

of a wake function or velocity defect law (Coles 1956) that adjusts for dynamics in the outer layer. The velocity profile across the layer is then represented by

$$\frac{U(z)}{u_*} = \frac{1}{\kappa}\left[\ln\frac{z}{z_0} + 2\Pi\sin^2\left(\frac{\pi}{2}\frac{z}{\delta}\right)\right]. \quad 13.$$

Here, Π is a flow-dependent wake strength parameter. For fully developed flow, δ is equal to h in Equation 13, and Π is approximately 0.2 (Nezu & Nakagawa 1993). The presence of a free surface can affect turbulent flow differently, suppressing vertical turbulent motions and modifying the velocity profile relative to that near the center line in a closed channel or at the upper edge of a developing boundary layer (see Talke et al. 2013). Guo & Julien (2006) developed a modified wake function that accounts for a near-surface reduction in velocity for open-channel flow.

If we consider C_D from Equation 9 defined using the depth-averaged velocity and assume fully developed flow and $k \ll h$ so that Equation 13 applies over the full depth, then the drag coefficient can be related to the hydrodynamic roughness as

$$C_D \approx \kappa^2\left[\ln\left(\frac{h}{z_0}\right) + (\Pi - 1)\right]^{-2}, \quad 14.$$

where the drag coefficient then varies as a function of depth, for a given roughness (Lentz et al. 2017).

Details and consequences associated with the logarithmic profile have been discussed extensively elsewhere (Grant & Madsen 1986, Jiménez 2004, Trowbridge & Lentz 2018). The validity of Equations 11–13 has been verified in multiple settings (Lueck & Lu 1997, Sanford & Lien 1999), although values of the shear stress derived from the law of the wall and measurements of the shear stress made using other means, e.g., from the variance method (Stacey et al. 1999), sometimes do not agree. Nonetheless, the law of the wall has two useful features. First, as is evident in Equation 14 and shown by Lentz et al. (2017), the dependence of drag coefficients for depth-averaged flows on h/z_0 can be obtained where roughness scales are assumed to be much smaller than the overall depth [similar results were observed by McDonald et al. (2006) for cases where the coral canopy was a sizable fraction of the total depth]. Second, as discussed below, the assumed eddy diffusivity variation with height appropriate to the law of the wall can be used with measurements of bulk concentration gradients of scalars, such as total alkalinity or temperature, to infer fluxes. In the context of coral reefs, however, several factors put the validity of Equations 11–13 into question, including large and highly heterogeneous roughness and the influence of surface waves.

3.2. Turbulence over Highly Irregular Roughness

The parameter P in the functional relation in Equation 10 represents some quantitative measure (or set of measures) of irregular reef roughness that captures the connection between the complex multiscaled surface and the hydrodynamic roughness z_0 in Equation 11. Several measures have been proposed in engineering studies of rough boundaries, including rms height, spectral moments, and roughness slope, among others (see Schultz & Flack 2009 and references therein). As summarized by Schultz & Flack (2009, p. 1), "Even with modest success of these correlations for a specific roughness type, it can be concluded that, at present, there is no sufficiently satisfactory scaling for a generic, three-dimensional roughness." The situation is more acute when considering complex roughness associated with coral reef canopies.

We can nonetheless obtain some guidance on how to approach roughness parameterization by considering regular roughness arrays. Considering a single bluff body of height k and transverse

width s on a flat bottom within a steady mean flow U, the total pressure drag should be well described using a drag coefficient of order 1 and using the frontal area ks. If we consider a regular array of these elements, sparsely spaced at intervals of w and b in the longitudinal and lateral directions, respectively, then the total drag per unit area is

$$\frac{D}{A_T} \sim \rho U^2 \frac{ks}{b\mathrm{w}} \sim \rho U^2 \lambda, \qquad 15.$$

where λ represents the roughness density, or the frontal area of elements per plan area. Following this paradigm, it seems reasonable that the force exerted on the boundary, and, by corollary, the hydrodynamic roughness, should be proportional to the exposed frontal area. For two-dimensional beds, this regime is described as k-type roughness, where the hydrodynamic roughness is a function of the height of elements, k, and the roughness density, λ (Perry et al. 1969). Measurements show that z_0/k is linear with λ for $\lambda \leq 0.15$ (Raupach et al. 1991, Jiménez 2004). Since $\lambda \sim k/\mathrm{w}$, this points to the aspect ratio of the roughness elements, or the roughness slope, as a relevant parameter, as observed for sand ripples (Nielsen 1992). Engineering studies have similarly shown slope to be relevant for drag (Napoli et al. 2008, Schultz & Flack 2009).

Roughness slope has been used successfully to describe drag for reef surfaces. Rogers et al. (2018) used a numerical model to examine flow over a reef surface obtained from high-resolution topographic measurements from a shallow reef flat in American Samoa with relatively sparse coral coverage. Model drag estimates agreed well with observed values and were well predicted using Equation 14 with z_0 based on rms roughness and an average roughness slope.

For the regular roughness case, as element spacing is reduced, flow sheltering begins to play a role, reducing the relative flow velocity and complicating the relationship with λ. When spacing is reduced so that $k \sim \mathrm{w}$, the full element height k is no longer relevant for drag. This is the δ-type roughness regime identified by Perry et al. (1969). Leonardi et al. 2003 showed that for $\mathrm{w} < 5k$, the hydrodynamic origin approaches ~0.1w below the top of the roughness elements. This can be interpreted as a critical cavity aspect ratio $\mathrm{w}/k \sim 5$, below which the outer flow no longer responds to the lower part of the cavity geometry. For δ-type roughness, then, the full roughness density is no longer relevant in Equation 15, and the roughness element spacing w must play a role in setting the hydrodynamic roughness.

Rajagopalan (2010) applied the critical cavity aspect ratio paradigm to two-dimensional irregular roughness to determine the hydrodynamic origin ζ_0 relative to the top of the roughness, based on an effective cavity aspect ratio for the irregular bed. For the two-dimensional case, the hydrodynamic roughness was given by $z_0 \sim \zeta_0(1 - \lambda_{\zeta 0})$, where $\lambda_{\zeta 0}$ is a modified roughness density measured down to ζ_0. This idea is consistent with an alternate empirical roughness density λ_s that adjusts for the windward wetted surface area (Sigal & Danberg 1990, van Rij et al. 2002). Numerous relationships between z_0 and λ and between z_0 and λ_s have been determined empirically for a range of two- and three-dimensional bed geometries, as reviewed by Flack & Schultz (2010).

As noted above, coral reefs are commonly multiscaled (Zawada & Brock 2009, Duvall et al. 2019), with roughness distributions that can be described by a red spectral distribution (Nunes & Pawlak 2008, Jaramillo & Pawlak 2011, Amador et al. 2020) over a range of scales spanning O(10 cm) to O(10 m). To resolve the relevant spectral range, Reidenbach et al. (2006) covered a section of reef with plastic sheeting, effectively eliminating fine-scale roughness, and found that drag and turbulence were unchanged. The Eilat forereef they considered (**Figure 2*b***) could be described as a sparse canopy with a set of isolated obstacles with $k/b \gg 1$, so results may not be broadly applicable to more dense canopies, but their observations suggest that the larger roughness scales are dominant in the mean flow drag response.

At the lower end of the spectrum, the transition between the scales that contribute to roughness and those that can be considered bathymetry is not obvious for reef topography. Conceptually, we might consider scales that lead to flow separation as contributing to roughness, with longer length scales driving a potential flow response. Schultz & Flack (2009) noted that roughness with an average slope less than 0.35 did not map onto the hydrodynamic roughness, denoting lower slopes as wavy surfaces. Spatial drag measurements by Amador et al. (2020) over a sparsely covered forereef were best correlated with spectral roughness rms for wavelengths greater than 20 m (for depths of 5–30 m), suggesting that the larger roughness scales were most relevant in determining drag, consistent with the results of Reidenbach et al. (2006). The apparent discrepancy between these results and Schultz & Flack's (2009) critical slope may be associated with the fact that, for coral reefs, longer wavelengths are more likely coincident with sharp changes, as for spur-and-groove topography (Storlazzi et al. 2003), that are manifested in broad spectral distributions.

Where water depth is much greater than the roughness height, $k \ll h$, we can explore whether the overlying flow can be at least in local equilibrium with the local bed roughness. Studies of rough wall turbulence have shown that the boundary layer thickness must satisfy $\delta/k_s > \sim 40$, where k_s is the equivalent sand grain roughness, for the turbulence similarity assumptions that underlie Equation 11 to be valid (Jiménez 2004, Flack et al. 2005). Where this condition is not met, turbulence may be more characteristic of that for flow over obstacles. Nevertheless, velocity profiles are well described by logarithmic structure in many high-roughness coral reef environments and yield bed stresses that agree with other methods (Reidenbach et al. 2006, Lentz et al. 2017, Arzeno et al. 2018, Amador et al. 2020). Spatially averaged drag estimates by Amador et al. (2020) yielded values that compared reasonably well with log fit and Reynolds stress estimates at one of two fixed sites. At a second site, where advection was notable, the comparison was poorer. At both sites, however, Reynolds stress profiles showed a relatively weak connection with local shear, indicating nonequilibrium conditions (A. Amador, S.N. Giddings & G. Pawlak, manuscript in review).

The high spatial heterogeneity that characterizes coral reef environments poses a challenge for interpreting field observations traditionally obtained from a single location. It also represents a practical problem for numerical modeling where model grid cells require averaging over variable roughness. These issues are similar to those associated with atmospheric flow over variable topography, and associated studies can provide some guidance in understanding turbulence in coral reefs. Meteorologists use the blending height δ_b as a measure of the vertical extent at which effects of surface heterogeneities are no longer discernible (Mahrt 2000). Mason (1988) described the blending height as the level at which a change in bed stress is balanced by a corresponding perturbation in advection, which gives $\delta_b = C_b L_c (u_*/U_{\delta_b})^2$, where L_c is a characteristic horizontal scale for heterogeneity, U_{δ_b} is the velocity at the blending height, and C_b is a constant of order 1. Alternately, the blending height has also been defined using a diffusive length argument (Claussen 1990) as $\delta_b = C_b L_c (u_*/U_{\delta_b})$. The blending height can be interpreted as the height above a homogeneous patch of roughness to which the flow can be considered in local equilibrium. For coral reef flows with depth h and typical steady-flow drag coefficients $C_D \sim 10^{-2}$ (Lentz et al. 2017), these relations suggest that heterogeneity at scales less than $L_c = 10$–$100h$ will lead to turbulence that is not in equilibrium with the local roughness. Given the roughness regimes represented in **Figure 2**, we can anticipate that spatial variability will affect turbulence for many reef environments. In these cases, local advective contributions to momentum balances and to turbulent fluxes will be important.

Spatial variability brings about additional complications in parameterizing turbulent stresses over reef scales due to the role of persistent spatial flow structure. As shown by Mahrt (1987) for numerical modeling of atmospheric flow, this spatial structure contributes to subgrid fluxes that appear via the dispersive stress in Equation 8. For coral reefs, specific mechanisms for spatially

variable, persistent flow can include local advection and acceleration around individual roughness elements and reef topography (Hench & Rosman 2013, Rogers et al. 2015), wave-induced residuals (Pawlak & MacCready 2002), and thermally driven flows (Monismith et al. 2006, Molina et al. 2014).

Taylor (1987) discussed a similar issue in averaging of variable roughness, noting that the spatially averaged hydrodynamic roughness length is given by $\ln z_{0\alpha} = \langle u_* \ln z_0 \rangle / \langle u_* \rangle$. Using a Taylor series expansion, one can approximate this as $\ln z_{0\alpha} \approx \langle \ln z_0 \rangle$, which avoids averaging over the shear stress velocity. These relations highlight the complications that must be considered in interpreting local observations and in applying these to numerical models.

Extrapolating the approaches from atmospheric boundary layers neglects effects due to surface waves that are intrinsic for many reef environments. Wave effects on boundary layer structure in heterogeneous roughness have not previously been considered in detail.

4. SURFACE WAVES AND THE WAVE BOUNDARY LAYER

Surface waves drive oscillatory motions that can often be larger than steady flows in many reef environments (Monismith 2007). The effects of irrotational surface wave motion on turbulence generated by steady flow over the rough seabed is commonly neglected, although Teixeira & Belcher (2002) have shown that wave-induced strain and Stokes drift shear can result in time-variable modulation of Reynolds stresses and anisotropy. Near the bed, the periodic motions directly drive turbulence and indirectly modify the mean flow.

The vertical extent of the bottom boundary layer associated with wave-driven motions is limited by the wave period, so that vertical gradients in velocity along with corresponding stresses and turbulent intensities are of much higher magnitude than those for comparable steady flows (Grant & Madsen 1979). For sediment seabeds, wave boundary layer thicknesses are on the order of centimeters (Grant & Madsen 1986, Trowbridge & Lentz 2018). For rough beds, however, the turbulent wave boundary layer extent is determined by the height of the roughness elements, which for coral reefs can range from centimeters to meters (see **Figure 2**).

Similar to the thicker steady-flow boundary layer, turbulence within the wave-driven boundary layer can be related to the time-variable shear stress velocity. The magnitude of the corresponding time-varying stress is typically parameterized using a wave friction factor, f_w, as

$$\tau_{w_m} = \frac{1}{2} \rho f_w U_w^2, \tag{16.}$$

(Jonsson 1967). Extensive work has been carried out toward developing parameterizations for f_w over homogeneously rough beds with $k/A \ll 1$, primarily in the context of coastal engineering and sediment transport applications. The majority of these studies build on the original formulation by Jonsson (1967), later modified by Swart (1974) and examined experimentally by Kamphuis (1975), that shows an increase in f_w with increasing relative roughness k/A. More recent work by Dixen et al. (2008) has extended this result for large roughness where $k/A \sim O(1)$.

The dissipation of wave energy due to bed friction is associated with the component of the time-varying stress that does work on the oscillatory flow. Jonsson (1967) defined the wave energy dissipation factor f_e for sinusoidal waves based on the mean dissipation of wave energy, which is given by

$$\varepsilon_f = \overline{\tau_b u_w(t)} = \frac{2}{3\pi} \rho f_e U_w^3, \tag{17.}$$

where $u_w(t)$ is the time-variable free-stream wave velocity. Because the bottom stress is not generally in phase with the wave motion, f_e and f_w are not strictly the same, though they are often used interchangeably. Madsen (1994) related these formally for spectral waves as a function of their corresponding phase shift.

Nielsen (1992) reviewed several models for turbulent wave boundary layers over homogeneous roughness. A quasi-steady model, assuming a log profile as in Equation 11, agrees reasonably well with measured velocity profiles for low relative roughness ($k/A < 0.01$). For large roughness ($k/A > 0.06$), the boundary layer structure was well approximated using a vertically uniform eddy viscosity, consistent with wake-dominated turbulence (see Pope 2000).

The extension of results for wave boundary layers for homogeneous roughness to coral reefs is challenged by the broad range of coral bed morphologies. The dense canopies shown in **Figure 2** would suggest that coral reef surfaces may fall within high relative roughness values, k/A. As noted above, however, reef roughness is multiscaled, with roughness elements that also differ fundamentally from sand, gravel, and rock boundaries. Though some massive corals may be well described as solid obstacles, elements are commonly characterized at small scales by branching networks. As discussed below, the degree to which flow penetrates these elements is a function of wave frequency (Lowe et al. 2005c, Reidenbach et al. 2006), with high-frequency waves tending to generate greater flow through the elements. As with steady flow, the connection between physical roughness and the associated hydrodynamic roughness used for friction factor parameterizations is thus not clear.

Reef surfaces dominated by low-relief encrusting coral coverage may be well represented by wave boundary layer models with homogeneous roughness. Estimates of wave dissipation factors by Lowe et al. (2005a) over a reef flat with relatively uniform, low-relief roughness were well explained across a range of frequencies by a homogeneous-roughness parameterization using a single roughness scale. Estimates for f_e ranged from 0.1 to 0.7 for frequencies between 0.1 and 0.6 Hz, with higher values at higher frequencies, consistent with increasing friction and dissipation at higher relative roughness. The inferred roughness scale compared well with physical roughness measurements quantified using rms over 3-m transects. Other studies have yielded comparable estimates for dissipation factors, primarily for reef flats (Gerritsen 1981, Nelson 1996, Hearn 1999, Falter et al. 2004, Péquignet et al. 2011) and forereef environments (Gerritsen 1981, Bandet 2009, Péquignet et al. 2011, Monismith et al. 2013).

Péquignet et al. (2011) measured a higher friction factor ($f_e = 0.4$) for a forereef in Guam with complex, multiscaled roughness, relative to the reef flat ($f_e = 0.06$). Notably, Monismith et al. (2015) reported $f_e = 1.8$ for a Palmyra forereef, attributing the high dissipation to the complex canopy structure, which introduces an additional component to the drag, so that the wave dissipation factor, following Lowe et al. (2007), is given by

$$f_e = f_{e_0} + C_d \lambda \alpha_w{}^3, \qquad 18.$$

where f_{e_0} is the dissipation due to drag at the bottom, with typical values of 0.01–0.1; $C_d \approx 1$ is a drag coefficient associated with canopy structure; λ is the roughness density; and α_w represents the ratio of wave velocity within the canopy to the free-stream wave velocity. The factor α_w is dependent on wave frequency, estimated by Lowe et al. (2005b) as $0.5 < \alpha_w < 0.7$ for dense canopies and long waves.

The total stress on coral elements due to wave motion has three components: viscous shear stress, pressure drag associated with separated flow, and inertial forces (added mass effects) associated with flow acceleration. Yu et al. (2018) noted that these various components of forces lead to ambiguous definitions for the wave friction factor. As discussed above and also shown by Yu et al. (2018), viscous shear forces are generally negligible at the high Reynolds numbers characteristic

of reef environments. The inertial forces on roughness elements are dominant at high wave frequencies, while pressure drag dominates for longer waves and for steady flow (Lowe et al. 2005b, Yu et al. 2018). Because the inertial forces are associated with potential flow effects, they do not contribute to the stresses reflected in Equation 16 (see Warner & MacCready 2009). Furthermore, because they are in quadrature with the outer wave flow, they also do not contribute to f_e, as is evident in Equation 17.

The pressure drag on the elements, associated with the second component in Equation 18, is related to vorticity formation in the wave boundary layer and is then the dominant contribution to the stress within the fluid. Using the more general Reynolds decomposition in Equation 4 to account for wave motion, it is evident that the time-variable, phase-averaged vertical stress in the wave boundary layer will have two contributions:

$$\tilde{\tau}_{xz} = u'w' + \rho\tilde{u}\tilde{w} \qquad 19.$$

(Nielsen 1992). Sleath (1987) showed that the second term, associated with phase-coherent turbulent motions, was dominant for flow over rough beds, relating the associated fluxes to persistent jets and bursts generated by discrete roughness elements. Bandet (2009) used along-beam measurements from a horizontally profiling acoustic Doppler current profiler to resolve spatial patterns in phase-coherent motions in the outer region of the wave boundary layer over a 3-m section of forereef characterized by sparse, multiscale canopy elements (**Figure 3**) with a red spectral roughness distribution (Nunes & Pawlak 2008). Coral roughness elements in the vicinity of the measurements extended up to 30 cm above the substrate with an rms height of $k_{rms} = 16$ cm. **Figure 3** shows the phase-averaged vorticity, ω, normalized by U_w/k_{rms}. The data reveal a wave boundary layer that extends up to 50 cm above the substrate but with a phase structure that varies with wave orbital amplitude. Boundary layer thickness increases slightly with orbital amplitude but generally scales with roughness height. Single-profile measurements below the roughness (not shown in **Figure 3**) show that the near-bed phase is invariant with increasing orbital amplitude. Changes in the vorticity phase above the roughness height arise due to increased advection from the previous cycle as the oscillatory excursions increase, reflecting the influence of larger length scales as the orbital amplitude increases. These variations in phase-coherent vorticity thus alter the phase response for the turbulence and associated stresses in Equation 19.

The near-bed orbital amplitude provides a characteristic length scale for the wave motion that can provide some guidance in determining the range of scales that are hydrodynamically relevant for wave dissipation. For a red spectral distribution, this raises an interesting scenario where increasing orbital amplitudes statistically sample larger roughness scales such that $k = k(A)$. In this case, the ratio k/A will depend on the character of the roughness distribution.

Where roughness scales are comparable to the overall depth [$k/h \sim O(1)$], the wave boundary layer paradigm implicit in standard parameterizations for f_w is questionable. The drag formulation in Equation 18 may still provide a useful framework for estimating wave dissipation and boundary layer turbulence.

Wave-generated turbulence near the seabed and the associated increase in momentum transfer can modify turbulence in the steady flow, increasing u_* with decreasing U_c/U_w. Grant & Madsen (1979) devised an analytical model for $k \ll h$ based on a quasi-steady law-of-the-wall profile within the wave boundary layer that results in an increased apparent roughness in the steady-flow log profile in Equation 11. Numerous other models have been proposed using varying wave boundary layer turbulence closures for different wave–current flow regimes (see Fredsøe & Deigaard 1992). Christoffersen & Jonsson (1985) used a constant eddy viscosity in the wave boundary layer applicable for large roughness. These models have not been evaluated for large multiscale coral reef roughness.

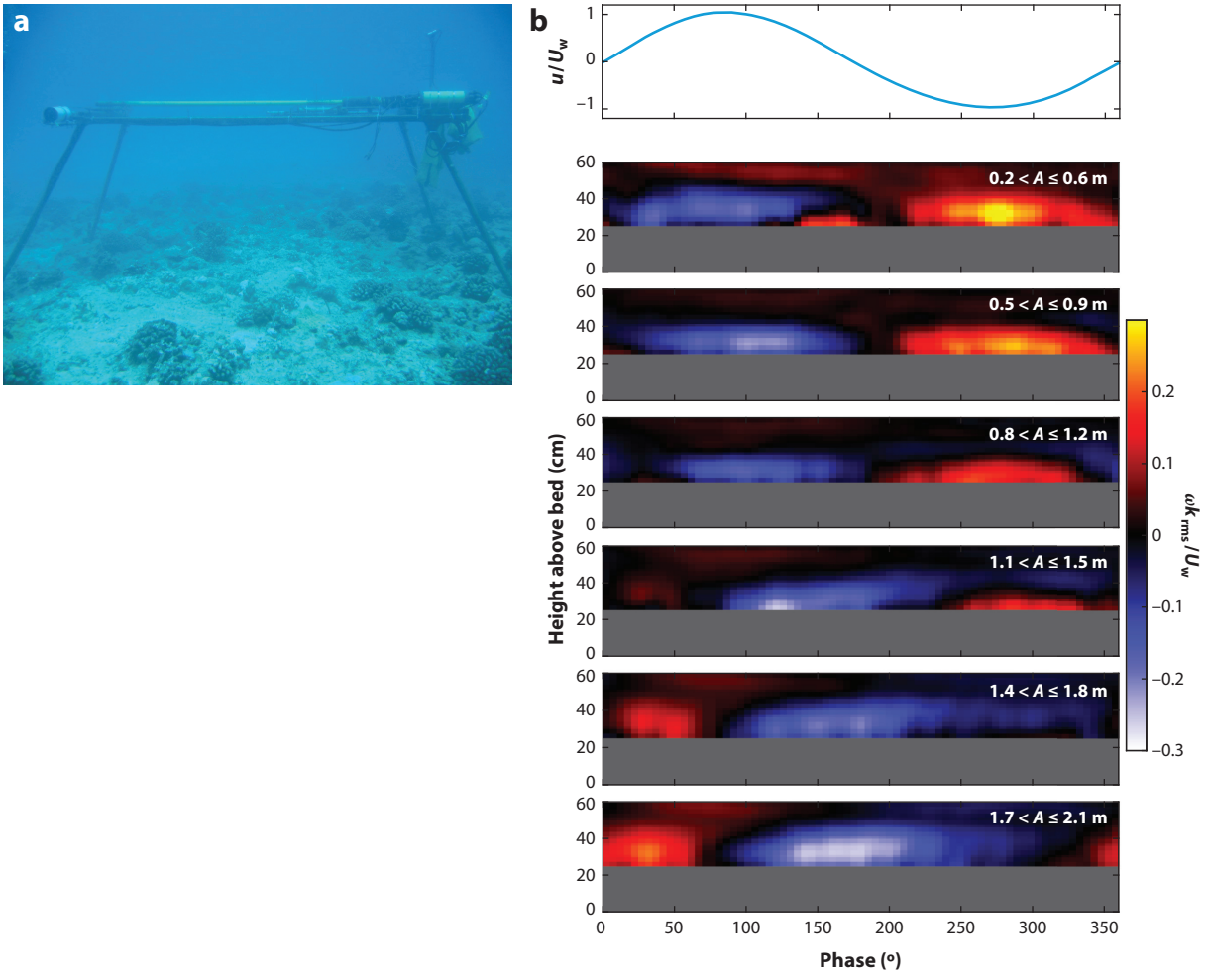

Figure 3

(*a*) Bed profiler. Panel adapted from Bandet (2009). (*b*) Phase-averaged wave boundary layer structure over the rough coral reef surface shown in panel *a*. The top subpanel shows cross-shore normalized wave velocity (60 cm above the bottom). The six lower subpanels show near-bed normalized spatially averaged vorticity versus average height above bed over a 2-m transect for increasing wave orbital amplitude, A.

Lentz et al. (2018) followed a simpler approach to account for wave effects on steady flow over a reef flat following the bed stress formulation considered by Wright & Thompson (1983) and Feddersen et al. (2000):

$$\tau_{\mathbf{b}} = \rho C_D \overline{(\overline{\mathbf{u}} + \widetilde{\mathbf{u}})\,|\overline{\mathbf{u}} + \widetilde{\mathbf{u}}|}, \qquad 20.$$

where the vector bed stress is determined from the time average of the instantaneous stress. This estimate for the steady stress effectively accounted for variations in U_c/U_w for a given drag coefficient or hydrodynamic roughness. Effects due to variations in the relative angle ϕ_{wc} between waves and currents are included implicitly in Equation 20 since it is based on the velocity vectors. Grant & Madsen's (1979) model showed that ϕ_{wc} had only small effects on the mean stress, though this has not been exhaustively verified. Equation 20 is similar to the linear drag law used

by Hearn (1999), where the quadratic velocity factor in Equation 9 is replaced by a steady velocity scale multiplied by a factor proportional to the wave motion.

For highly spatially variable reef topography, wave motion can drive further spatial variability in turbulence. Pawlak & MacCready (2002) showed that oscillating flow over inhomogeneous roughness can drive strong residual flows, related to the periodic jets and bursts noted by Sleath (1987) in wave boundary layers. These residuals then contribute to the total near-bed steady stress via the dispersive term $\langle \bar{u}'' \bar{w}'' \rangle$ in Equation 8.

5. COMPLICATIONS TO THE STANDARD ROUGH BOUNDARY MODEL

It is clear that, as in many inner shelf and coastal flows, the law of the wall (albeit including modifications to account for surface waves) is the fundamental model for vertical flow structure over coral reefs. Yet several important aspects of these coral reef flows can significantly affect the applicability of this law: the effects of stratification, either preexisting or due to internal waves (Davis & Monismith 2011); the effects of shallowness of the flow, i.e., the fact that the free surface can influence the largest scales of motion (Walter et al. 2011); and the effects of turbulence produced by breaking surface waves (Huang et al. 2012).

In their study of turbulence on a reef for $h_c/h \ll 1$ (**Figure 2**), Davis & Monismith (2011) showed that, in the absence of stratification, turbulence properties such as the turbulent kinetic energy dissipation rate behaved as would be expected from the law of the wall. By contrast, in the presence of shoaling internal tides, a common feature of the field site (Leichter et al. 1996, Davis et al. 2008), stratification significantly altered the vertical structure of the flow—for example, producing velocity profiles with near-bed maxima, behavior that is decidedly different from Equation 11. Accordingly, turbulence quantities such as Reynolds stress profiles and turbulent kinetic energy dissipation rate were quite different from what would be expected for the classical rough wall flow. In this case, attempts to use law-of-the-wall velocity fits to find u_* and thus the scalar diffusivity, K_t, would contain significant error.

Free-surface effects may also significantly affect the applicability of the law of the wall to coral reef flows. First, while there do appear to be approaches for modeling how waves modify shallow flows (see above), there has never been an assessment of how waves modify scalar fluxes. As shown by Lowe et al. (2005b, 2008), wave motions in the canopy behave very differently from mean flows in that they tend to be much less damped by drag, since for waves the fundamental force balance tends to be between accelerations and pressure gradients. One effect of this is that mass transfer in the presence of waves tends to be somewhat greater than would be expected solely on the basis of the inferred drag (Falter et al. 2005, Lowe et al. 2005c). Thus, it seems unlikely that u_* inferred from log fits of flows over reefs in the presence of the waves can be used without modification to infer scalar fluxes. Second, it is well known that turbulence produced by breaking waves behaves quite differently from turbulence produced by bottom boundary layer drag (Terray et al. 1996, Jones & Monismith 2008). Thus, given that regions of wave breaking and thus high mass transfer (Hearn et al. 2001) may be important to the overall functioning of any given reef, wave breaking may play a significant, albeit virtually unstudied, role in the overall functioning of reef ecosystems.

Finally, a subtler aspect of the presence of the free surface is its potential for modifying large-scale turbulence structures that are important to fluxes of any quantities, i.e., either of momentum or of scalars. As seen in the canonical cospectra described by Kaimal et al. (1972), as applied to coral reefs, roughly 50% of the stress is carried by eddies with horizontal scales larger than the depth. Measurements reported by Walter et al. (2011) for tidal flow in a shallow estuary are likely similar to what might be found for shallow reef flows. They found that their cospectra generally matched the form of Kaimal et al.'s cospectra, differing most significantly at small wavenumbers,

i.e., for scales comparable to or larger than the depth of the flow. This may be an effect of the free surface in that large scales of turbulence must do work against gravity to deform the free surface (e.g., Pan & Banerjee 1995). Whether these free-surface effects are large enough to be of practical interest in terms of influencing overall drag and mass transfer remains to be determined.

6. WITHIN-CANOPY FLOWS

Above, we have examined approaches for characterizing and quantifying structural complexity to understand its effect on the flow above the reef, but we are also interested in the structure of flow and turbulence within the roughness sublayer of the coral reef canopy, as this is a chemically and biologically active region where the mass flux of material at the water–coral interface controls many important ecological processes (Section 7).

Foundational theoretical and observational work has been done in terrestrial and aquatic canopies such as forests (Raupach & Thom 1981, Finnigan et al. 2009, Belcher et al. 2012) and seagrass beds (Nepf & Vivoni 2000; Ghisalberti & Nepf 2002, 2006; Nepf 2012). These studies provide a conceptual framework for our understanding of flow in coral reef canopies. Within a canopy, flow encounters roughness elements, and the forces acting on the surfaces of these elements dissipate kinetic energy and remove momentum from the flow. The net result is enhanced drag on the mean flow within the canopy. That this drag is extended over a vertical region ($\sim h_c$) and not just on a surface plane is what distinguishes canopy flows from more familiar boundary layer flows (Finnigan 2000).

For deeply submerged or unconfined canopies ($h_c/h < 0.1$) of sufficient roughness density, the discontinuity in form drag between the canopy and the region above results in an inflection point in the velocity profile (Finnigan 2000, Nepf 2012). This region of strong shear produces hydrodynamic instabilities characteristic of plane mixing layers where the turbulence is dominated by large coherent structures that transport momentum both into and away from the canopy (Raupach et al. 1996). Finnigan et al. (2009) performed large-eddy simulations of canopy flow and described the nature of the turbulent structures within a vegetated canopy as pairs of linked hairpin vortices (paired sweep and ejection) between which there is a pressure maximum and likely a scalar microfront. The prevalence of canopy-scale coherent structures means that turbulence in canopies is far from isotropic or random and that vertical turbulent transport is an important part of the turbulent kinetic energy balance (Raupach et al. 1996). Large coherent structures that penetrate the canopy from the free-flow region above break down quickly upon interacting with canopy elements, resulting in a spectral short circuit of turbulent energy to small-wavelength structures (Finnigan 2000). Additionally, within the canopy, turbulence is created at the scale of canopy elements as flow is forced to move around branches or blades, creating wakes.

Within unconfined canopies, the momentum balance is primarily between the shear stresses at the top of the canopy and the form drag exerted by the canopy elements (Raupach 1992). This shear-dependent momentum transfer results in a region of strong turbulence and rapid renewal of fluid from the top of the canopy down to the penetration depth of the coherent structures, but below this region, flow is reduced and turbulent mixing is weak (Nepf & Vivoni 2000, Ghisalberti & Nepf 2006). However, when the canopy takes up a larger fraction of the total water column ($0.2 < h_c/h < 1$), as in seagrass beds in shallow coastal waters, the external pressure gradient also becomes a significant force driving flow within the canopy (Nepf 2012). The degree of canopy submergence determines the relative importance of shear stresses and pressure gradient forces within the canopy. As h_c/h approaches unity, the shear layer at the top of the canopy disappears, and flow within the canopy, driven entirely by external pressure gradients, is greater in magnitude and more vertically uniform than it is in unconfined canopies (Nepf & Vivoni 2000).

There are some notable differences between coral canopies and their other aquatic or terrestrial counterparts. In terrestrial canopies, the flow problem is typically considered to be semi-infinite or unconfined ($h_c/h \ll 1$), but coral reefs are often in tidally influenced and shallow coastal environments; the height of the canopy can be a significant fraction of the depth of the water column, even emergent at low tide; and h_c/h is time variable. Another consequence of their shallow-water habitats is that surface gravity waves can drive oscillatory flow within coral canopies, enhancing exchange relative to unidirectional flows. Lastly, most of what we know about within-canopy flows is from studies considering idealized geometry or the uniform vertical and horizontal distribution of canopy roughness elements [although idealized studies of nonuniform roughness by Rominger & Nepf (2011) examined flow adjustments within a canopy]. However, the multiscale, multifractal complexity of coral reef structures results in spatially variable resistance, and this nonuniform structure can be important to within-canopy flow structure (Asher & Shavit 2019, Duvall et al. 2019).

Observations of mean and turbulent flow structure inside realistic coral canopies have been limited; laboratory studies (Reidenbach et al. 2007, Lowe et al. 2008, Asher et al. 2016, Asher & Shavit 2019), all of which used densely packed arrays of coral skeletons of *Pocillopora meandrina* or *Porites compressa* (both branching species), and one field study (Hench & Rosman 2013) (see **Figure 2*f***) of flow around bommies of *Porites rus* have reported measurements on canopy flows. Of these studies, those of Reidenbach et al. (2007) and Lowe et al. (2008) focused on comparisons of unidirectional and oscillatory flow dynamics within canopies, while those of Hench & Rosman (2013) and Asher & Shavit (2019) sought to understand the role of spatially variable canopy geometry.

Lowe et al. (2008) had some success adapting porous media flow theory to describe flow within a relatively homogeneous canopy of *Porites compressa* through the addition of a canopy shear stress term. This approach characterizes the canopy resistance as a laminar resisting force and form drag that are both dependent on a characteristic length scale of the porous medium, which is assumed to be homogeneous in space. However, the nonuniform spatial distribution of porosity and resistance within natural coral reef canopies can generate regions of strong flow accelerations, recirculation zones behind coral colonies, and interacting wakes (Hench & Rosman 2013). Persistent spatial variations in flow can contribute to the dispersive stress term that appears when the momentum equation is spatially averaged (Equations 7 and 8). In laboratory measurements of flow within a canopy of *Pocillopora meandrina* skeletons, Asher & Shavit (2019) found the dispersive stress to be the dominant stress term for $h_c/h = 1$ cases and more than half of the magnitude of the Reynolds stress for $h_c/h < 1$ cases. These results, as well as evidence from other studies of spatially nonuniform canopies (e.g., Böhm et al. 2013, Moltchanov et al. 2015), suggest that the inner geometry of corals may generate high dispersive stresses that are a significant part of the momentum balance. Furthermore, it is possible that in past work, unaccounted-for dispersive stresses may have been responsible for observed differences between bulk drag and shear stresses measured at one or a few locations near a reef boundary. Further work is needed here to better understand the role of nonuniform canopy roughness in the redistribution of momentum within reefs.

Reidenbach et al. (2007) carried out laboratory experiments examining the velocity and turbulence structure above and within a bed of nonliving *Porites compressa* skeletons under unidirectional and wave-dominated flow (**Figure 4**). Flow was measured with a two-dimensional laser Doppler anemometer, and mass transport was estimated using planar laser-induced fluorescence with rhodamine 6G dye applied to the surface of the corals. **Figure 4*a*** is an effective visualization of the role that turbulent structures play in mass transport at the coral canopy–water interface. The rms horizontal velocity ($U_{\mathrm{rms}} = \sqrt{\langle u^2 \rangle}$) provides a comparable velocity scale for both unidirectional and oscillatory flows and is shown in **Figure 4*b***. Measurements of velocity and turbulence during unidirectional flow conditions (blue lines in **Figure 4*b*,*c***) exhibit some features characteristic of

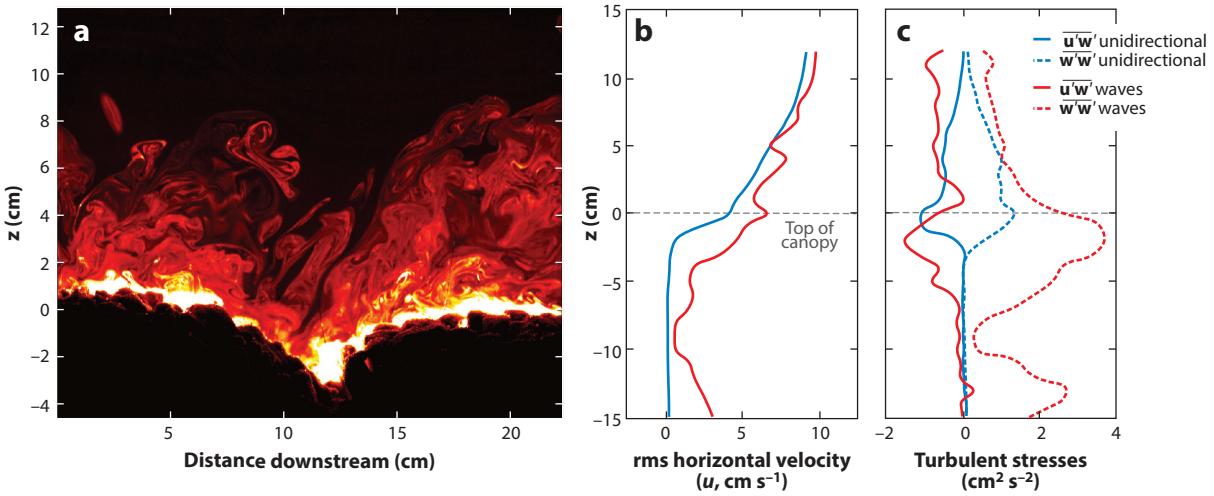

Figure 4

(*a*) Turbulent structures visualized with planar laser-induced fluorescence in a region at the interface between a canopy of *Porites compressa* coral skeletons in an oscillatory flow. (*b*) Root-mean-square (rms) horizontal velocity for a unidirectional flow run with a mean downstream flow of $U_c = 8.5$ cm s^{-1} (*blue lines*) and a wave-dominated flow with wave period $T = 5$ s and wave orbital velocity amplitude $U_w = \pm 9$ cm s^{-1} (*red lines*). (*c*) Turbulent stresses ($\overline{u'w'}$ and $\overline{w'w'}$) measured within and above a coral canopy. Figure adapted from Reidenbach et al. (2007) with permission from AIP Publishing.

canopy flows—very weak flow within the canopy and near-zero turbulent stresses (-15 cm $< z <$ -2 cm), an inflection point in the velocity profile at the top of the canopy and a corresponding peak in turbulent stresses ($z = 0$), and a logarithmic velocity profile and constant-stress region apparent above the canopy (1 cm $< z <$ 6 cm). In wave-dominated runs (red lines in **Figure 4*b*,*c***), rms horizontal velocity is still reduced within the canopy, but rms vertical velocity (not shown) is 50% higher within the canopy compared with the overlying fluid. Turbulent stresses in the wave-dominated flow peak just below the top of the canopy ($z = 2$ cm) and are nonzero and variable throughout the canopy, especially $\overline{w'w'}$. A wave boundary layer of thickness $\delta_w = 2.5$ cm was observed just above the canopy ($z = 0$–2.5 cm). While the magnitude of the velocities in the unidirectional and oscillatory flows were similar ($U_{rms} = 9.0$ cm s^{-1}), the increased turbulent energy in the wave-dominated run resulted in approximately twice the effective mass transfer (estimated both from planar laser-induced fluorescence analyses and using gypsum dissolution as a proxy for mass exchange) (Reidenbach et al. 2007). Some of this enhanced mass transfer is attributed to vortex ejections, identified from pulses of dye originating at the coral surface and emerging into the flow region above, which occurred repeatedly at the same phases of the wave, 150° and 270°.

7. BENTHIC FLUXES TO SUPPORT ECOSYSTEM FUNCTION

One of the primary motivations for the study of turbulent flow over and within coral reefs and other aquatic and terrestrial canopies has been to understand the physical processes governing the exchange of momentum, heat, and mass (i.e., nutrients, waste products, larvae, and disease) between the fluid above and the biologically active surface at the bed (Falter et al. 2013, Raupach & Thom 1981). Benthic marine communities, such as coral reefs, rely on the flow of water and turbulent mixing to sustain many biological processes, and this has been supported in many observational studies.

In a pair of noteworthy papers, Bilger & Atkinson (1992) and Atkinson & Bilger (1992) were the first to remark the importance of turbulent mass transfer to coral reef biogeochemistry and ecology. They were able to show that the uptake of phosphate by the reef community on the reef flat of Kaneohe Bay, Hawaii, was mass transfer limited, i.e., that this uptake rate was physically controlled by turbulent mixing between the reef benthos and the overlying water column. Mass transfer limitation is well known in the engineering literature, where, for example, it is important to the design of heat exchangers. These studies were able to show that experimentally determined engineering parameterizations of the flux of a scalar, F, from a rough boundary, represented in terms of a mass transfer velocity, V_t, with $F = V_t\,\Delta C$, where ΔC is the concentration difference between the surface and the fluid above (e.g., Dawson & Trass 1972, Dipprey & Sabersky 1963), could be applied to the Kaneohe Bay reef. These models take the form

$$\frac{V_t}{U} = f\,(\mathrm{Re_h}, k_s, \mathrm{Sc}), \qquad 21.$$

where U is an appropriate mean velocity scale; $\mathrm{Re_h} = Uh/\nu$ is the Reynolds number defined in terms of U and h, the outer length scale for the flow (e.g., the depth); k_s is the sand grain roughness; and Sc is the Schmidt number. However, one adjustment, an extra multiplicative factor of 6.4, was needed to fit the standard model to the reef observations. The authors suggested that this was because coral reefs have substantially more surface area for exchange per unit area of wall surface. Of course, one complication with this interpretation is the fact that, as shown in **Figure 5**, there can be enormous variability in local mass transfer rates over the entire surface of a single coral colony (Chang et al. 2013).

The physics of convective mass transfer offers an explanation for the behavior seen in **Figure 5** and the parametric dependence of the mass transfer velocity. In the absence of any flows, mass transfer would take place purely by molecular diffusion, whereas in the presence of flows, there is a very thin boundary layer near the surface across which diffusion sustains a flux. The thinner this layer is, the larger the diffusive mass flux is. For a flat plate or a wall—the case commonly of engineering interest—the thickness of the diffusive layer is determined by the flow away from the wall. As the velocity increases, the diffusive layer thins, and thus the mass transfer increases. However, for isolated objects, mean velocity strain can be an important determinant of local mass transfer. For example, mass transfer on a cylinder is maximal at the forward stagnation point, where the velocity is zero but the compressive strain is maximal, and minimal in the wake on the rear of the cylinder (Goldstein & Karni 1984, Sanitjai & Goldstein 2004, Chang et al. 2013). Thus, for a coral colony, mass transfer on parts of the colony facing into the flow are likely to be much higher than on rearward-facing parts. Moreover, because of reductions of velocity, wake interactions, and so on, as seen in the magnetic resonance velocimetry measurements of Chang et al. (2009), mass transfer rates would also be much smaller on the interior parts of a branching coral colony than on the tips of the branches.

To examine coral colony mass transfer behavior in detail, Chang et al. (2014) carried out large-eddy simulations of steady and oscillating flows through four different branching corals (one of which was the coral shown in **Figure 5**). A striking finding of this work was that local mass transfer rates, including those that were wave phase dependent, were strongly correlated with the tangential component of the local wall shear stress and not with the local pressure force, suggesting that colony-scale mass transfer might not be well parameterized by drag. Following the same approach as Chang et al. (2014), Stocking et al. (2018) used large-eddy simulations to study flows and mass transfer around massive (e.g., hemisphere-like) coral morphologies. They found that there could be subtle trade-offs between increasing surface area for mass transfer by increasing roughness and the concomitant reduction in local heat fluxes. These results should all be treated with some

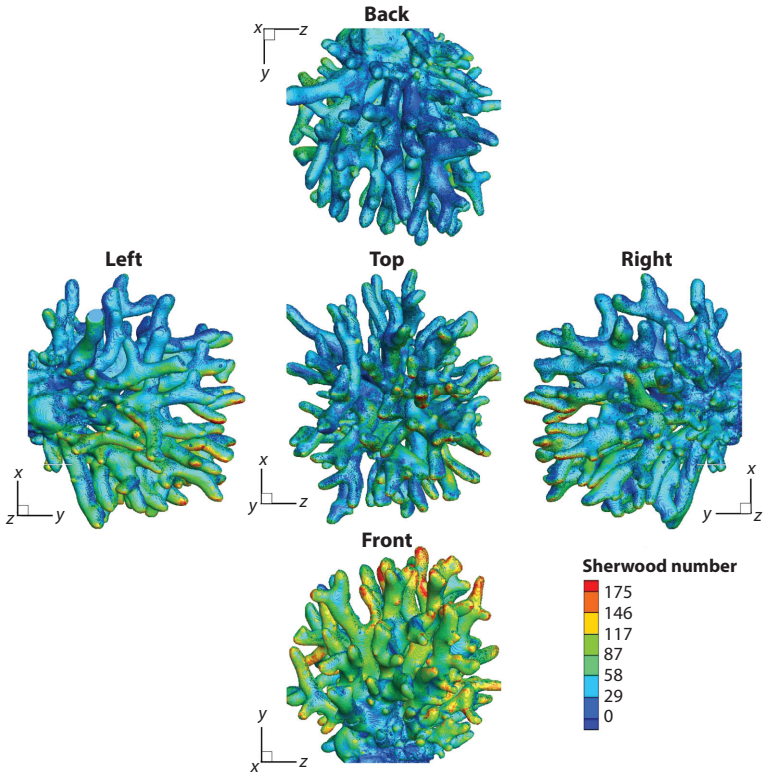

Figure 5

Local mass transfer (normalized by diffusive transfer rate, as the dimensionless Sherwood number) for a *Stylophora pistillata* colony immersed in a steady flow in a flume. Figure adapted from Chang et al. (2013) with permission from Springer Nature.

element of caution, however, since (*a*) both sets of calculations were done with Sc = 1, and the behavior of mass transfer for Sc ≫ 1 (characteristic of all scalars of interest) can differ significantly between small Sc and large Sc (Yaglom & Kader 1974), and (*b*) given that mass transfer is strongly affected by the details of the near-wall flow, computed fluxes can depend on details of the calculation method and on near-wall grid resolution.

Understanding flow effects at the reef scale requires knowledge of the integrated effect of the highly variable local mass transfer. This was explored by Falter et al. (2016), who attempted to show how flat boundary models might be extended to include coral canopies. The starting point for this analysis was the full set of equations for drag and mass transfer given by, for example, Atkinson (1992). These equations show that generally $V_t \propto U^{0.8}$, with a weak dependence on Sc. Falter et al. (2016) argued that the velocity dependence derived from rough wall experiments could be generalized to canopy flows by noting that the rough wall data give $V_t \propto \tau_b{}^{0.4}$, where τ_b is the wall stress. Thus, for canopy flows, one needs to consider the effective wall stress associated with the drag on the canopy elements averaged over the entire surface (Nepf 2012). Importantly, this drag and mass transfer depends on the velocity inside the canopy, which is itself a function of the free-stream velocity and the canopy density and geometry. Reanalysis of the mass transfer measurements of Lowe et al. (2005c), using as a velocity scale a hybrid velocity computed from the mean and wave velocities, showed good agreement with the $\tau_b{}^{0.4}$ dependence, although this result

is very much dependent on using the Reynolds number and canopy element density parameterization of Tanino & Nepf (2008), which do not account for unsteady drag effects, as documented by Sarpkaya (1975). Likewise, the single-colony calculations of Chang et al. (2014) suggest that the relationship between drag (primarily associated with separation and thus pressure forces) and mass transfer (associated with near-wall shear and strain) may not be robust. Nonetheless, this formalism has been used with some success to estimate mass transfer–limited nutrient fluxes on reefs other than Kaneohe Bay (Falter et al. 2012, Wyatt et al. 2012, Gruber et al. 2019).

It also appears that coral bleaching may involve mass transfer limitation: Nakamura & van Woesik (2001) showed that bleaching at high water temperatures could be suppressed if flows were sufficiently strong. The mass transfer interpretation of this result relies on the possibility that bleaching is designed to prevent the buildup of oxygen produced by symbiont photosynthesis in the polyps' tissue (Lesser 1997); high rates of mass transfer may enable the polyps to maintain nonharmful oxygen concentrations in their tissue. Given the strength of this result, it is surprising that few bleaching studies include flow measurements.

Besides transfer of nutrients, flow and thus turbulent mixing are also important to several other aspects of reef function: reef heterotrophy and larval settlement. While it is known that flow can increase coral heterotrophy by increasing the supply of zooplankton to the corals (Sebens et al. 1997), flow may also increase the flux of phytoplankton and other organic material to reef organisms (Genin et al. 2009, Ribes & Atkinson 2007). Assuming law-of-the-wall mixing (but with u_* measured directly) and using measured profiles of chlorophyll *a*, Monismith et al. (2010) calculated rates of phytoplankton grazing by a reef in the Florida Keys dominated by soft corals and sponges, finding that grazing rates increased with increased flows and thus turbulence.

A similar use of the law-of-the-wall mixing model is also the basis for the Benthic Ecosystem and Acidification Measurement System (BEAMS) approach devised by Takeshita et al. (2016) to measure fluxes of total alkalinity and thus the rate of net community calcification. This approach assumes (*a*) that the eddy diffusivities of scalars (K_t) and of momentum (ν_t) are the same, (*b*) that by fitting of Equation 11 to observed velocity profiles, one can estimate u_*; and (*c*) that, with u_* known, $K_t = \kappa u_* z$. Using these assumptions, fluxes of the scalar of interest can be estimated from profiles of scalar concentration C (see Monismith et al. 2010), i.e.,

$$F = -K_t \frac{\partial C}{\partial z}. \qquad 22.$$

As discussed above, while logistically convenient, this approach is limited to cases where surface wave motions are minimal and where the law of the wall can be taken to be reasonably accurate, i.e., when the water column is unstratified. In the presence of stratification, vertical velocity shear can be increased because vertical mixing is suppressed by stratification (Turner 1973). By contrast, Teneva et al. (2013) estimated K_t by combining measurements of turbulence dissipation, ε, and buoyancy frequency, N, with the stratified turbulence parameterization of Shih et al. (2005).

The potential effects of stratification would seem to be particularly important for reefs that experience episodic internal waves (Wolanski & Delesalle 1995, Leichter et al. 2006, Reid et al. 2019), because during internal wave events, when the water column stratification is due to the presence of internal waves (Davis & Monismith 2011), concentrations of particulates and nutrients can be substantially higher than they are when internal waves are not present (e.g., Leichter et al. 1996). How stratification affects mixing and turbulence is the subject of much ongoing research (see, e.g., Ivey et al. 2008, Gregg et al. 2018, Monismith et al. 2018) and is beyond the scope of the present review to describe in detail.

The extent to which Equation 22 can be used in the presence of surface waves is unknown. The fundamental challenge is that flow behavior in the presence of waves is fundamentally

different from that of steady flows. As documented by Reidenbach et al. (2007), there can be a strong phase dependence of vertical mixing of scalars. Moreover, turbulent kinetic energy production can be negative in some phases, as a result of large time-varying strains associated with wave motion (Teixeira & Belcher 2002). One practical effect of this behavior is that negative turbulent kinetic energy production implies negative eddy viscosities. Given the challenges of making eddy correlation measurements of fluxes (e.g., Long et al. 2019), it might be hoped that the time-averaged effects of this phase-dependent flow behavior is still describable by Fickian diffusion, i.e., by an eddy diffusivity, ideally one derivable from something like the law of the wall modified for the presence of waves (e.g., Grant & Madsen 1979).

Turbulence is also an important consideration for larval settlement on reefs. In a noteworthy laboratory study of wavy turbulent flow over a dense bed of coral skeletons (*Porites compressa* from Kaneohe Bay), Reidenbach et al. (2009) showed that the probability of larval settlement on a reef was dependent on the detailed statistics of the near-reef velocity field produced by both turbulence and waves. The reason for this was that larval settlement requires a short period of time during which the hydrodynamic forces on the larvae are sufficiently small for the larvae to explore and attach themselves to the substrate. Thus, what matters is the probability that the near-reef velocity remains sufficiently small for attachment to take place. Using measured velocities, the authors suggested that the probability of attachment dropped to zero for attachment times longer than about 10 s, although given much weaker velocities inside the coral canopy itself, the probability that a larva could successfully attach increased substantially. Extension of their results to reef structures other than densely packed *Porites compressa* skeletons remains to be done.

Most of the work considering mass transport to coral reefs has examined how aspects of the flow environment and canopy morphology act to passively modify exchange through the diffusive boundary region. However, there is some evidence that corals may be able to actively enhance mass transport by using their epidermal cilia to induce counterrotating vortices that break down the molecular diffusive region (Shapiro et al. 2014). The significance of vortical ciliary flows has not been demonstrated for a wide range of flow conditions but could be particularly important for shaping the microenvironment at coral surfaces under conditions of very low flow within a coral canopy.

8. A TURBULENT FUTURE FOR CORAL REEFS

The rich literature of turbulent properties in and above rough boundaries from the engineering literature (as reviewed above and in Jiménez 2004, 2012) and in terrestrial canopies (Raupach & Thom 1981, Finnigan 2000, Belcher et al. 2012) benefits our understanding of turbulence and flow in coral reef habitats, but, despite the apparent similarities, some common characteristics of coral reefs make the prediction of turbulence in this environment very challenging. Bedforms and canopy roughness within natural coral reefs are inherently multiscaled and even directionally dependent (e.g., the spur-and-groove formations in Rogers et al. 2015; other examples are given in Reidenbach et al. 2006, Arzeno et al. 2018). Some promising sensing technologies are emerging to help quantify this complex roughness (e.g., Chirayath & Earle 2016, Ferrari et al. 2016), and we are seeing some progress in the characterization of these structures through multifractal metrics (e.g., Duvall et al. 2019). However, recent evidence suggests that the nonuniform spatial distribution of porosity and resistance elements within natural coral reefs has a significant—and, in some cases, dominant—influence on the distribution of momentum within and above the coral canopy through the dispersive stress term (Asher & Shavit 2019). Waves also complicate turbulent dynamics on coral reefs. Oscillating flow over inhomogeneous roughness can induce strong, spatially varying residual flows that also contribute to dispersive stress terms. Dispersive stress is

challenging to measure because it requires spatially resolved turbulence measurements within a canopy, but its historical neglect may be responsible for the observed scatter between bulk drag estimates from flow above coral canopies and drag estimated from shear stresses at only one point (or a few points) in space (noted by Rosman & Hench 2011, Lentz et al. 2017). Future work should carefully consider the influence of spatial variations on the fluxes of momentum and scalars in interpreting observations in reef environments and in applying these to numerical models.

An improved understanding of turbulent processes on coral reefs is crucial for the prediction of momentum, energy, and scalar transport, as we have emphasized in this review. From an understanding of these basic fluxes, we can learn more about the physics that shapes reef ecosystem processes (Nakamura & van Woesik 2001, McClanahan et al. 2005, Nakamura et al. 2005), sediment suspension and transport (Pomeroy et al. 2015), and larval settlement on reefs (Reidenbach et al. 2009). Furthermore, we can begin to understand the physical–biological feedbacks inherent in reef ecosystems—not only how the canopy elements affect the flow and turbulent transport, but also how the physics shapes the growth and distribution of organisms within the reef canopy (see examples for other aquatic canopies in Luhar et al. 2008).

Understanding these complex feedbacks will become increasingly important if we are to effectively manage the climate-driven changes occurring in coastal ecosystems globally. The accelerating rise in ocean temperatures has led to multiple worldwide mass bleaching events and coral mortality in the last decade (Hughes et al. 2017). Calcifying reef organisms are the engineers of coral reef ecosystems, and thus, reduced rates of calcification and coral mortality are already resulting in system-wide changes in the architectural complexity of bed roughness and overall seafloor elevation due to biological and mechanical erosion (Bozec et al. 2015, Yates et al. 2017). Where corals struggle to survive, turf algae can become more abundant and, in addition to competing for space and light, can alter turbulence in the reef, reducing bed stress, which also implies the reduced mass transfer of necessary metabolites, such as oxygen and nutrients (Stocking et al. 2016).

Physics is key to the recovery of these ecosystems. The dispersal of coral gametes and settling of larvae, which provide the genetic material necessary for reef recovery or habitat redistribution, are determined as much by turbulence as by large-scale currents (Reidenbach et al. 2009). Additionally, coastal managers are exploring reef restoration as a strategy to protect shorelines from erosion due to ever-higher seas (Ferrario et al. 2014). An improved understanding of drag parameterization on reefs and the influence of wave-driven turbulence would benefit this effort.

DISCLOSURE STATEMENT

The authors are not aware of any affiliations, memberships, funding, or financial holdings that might be perceived as affecting the objectivity of this review.

ACKNOWLEDGMENTS

We are grateful for the many collaborations and conversations that have shaped our understanding of coral reef physics through the years, notably with Amatzia Genin and the late Marlin Atkinson. We would especially like to thank Jim Hench, Ryan Lowe, Johanna Rosman, Matt Reidenbach, Uri Shavit, and Jim Falter for fruitful discussions and contributing reef images for this review. K.A.D. and S.G.M. were supported in this work by the National Science Foundation (OCE-1753317 to K.A.D. and OCE-1948189 to S.G.M.). G.P. would like to acknowledge support from the National Science Foundation (OCE-1829993) and the Office of Naval Research (N00014-15-2-2303).

LITERATURE CITED

Amador A, Arzeno IB, Giddings SN, Merrifield MA, Pawlak G. 2020. Cross-shore structure of tidally-driven alongshore flow over rough bathymetry. *J. Geophys. Res. Oceans* 125:e2020JC016264

Arzeno IB, Collignon A, Merrifield M, Giddings SN, Pawlak G. 2018. An alongshore momentum budget over a fringing tropical fore-reef. *J. Geophys. Res. Oceans* 123:7839–55

Asher S, Niewerth S, Koll K, Shavit U. 2016. Vertical variations of coral reef drag forces. *J. Geophys. Res. Oceans* 121:3549–63

Asher S, Shavit U. 2019. The effect of water depth and internal geometry on the turbulent flow inside a coral reef. *J. Geophys. Res. Oceans* 124:3508–22

Atkinson MJ. 1992. Productivity of Enewetk Atoll reef flats predicted from mass transfer relationships. *Cont. Shelf Res.* 12:799–807

Atkinson MJ, Bilger RW. 1992. Effects of water velocity on phosphate uptake in coral reef-hat communities. *Limnol. Oceanogr.* 37:273–79

Bailey SC, Vallikivi M, Hultmark M, Smits AJ. 2014. Estimating the value of von Kármán's constant in turbulent pipe flow. *J. Fluid Mech.* 749:79–98

Bandet M. 2009. *Dynamics of wave-induced boundary layers over very rough boundaries: field observations over a stretch of coral reef*. PhD Thesis, Univ. Hawaii, Honolulu

Belcher SE, Harman IN, Finnigan JJ. 2012. The wind in the willows: flows in forest canopies in complex terrain. *Annu. Rev. Fluid Mech.* 44:479–504

Bilger RW, Atkinson MJ. 1992. Anomalous mass transfer of phosphate on coral reef flats. *Limnol. Oceanogr.* 37:261–72

Böhm M, Finnigan JJ, Raupach MR, Hughes D. 2013. Turbulence structure within and above a canopy of bluff elements. *Bound. Layer Meteorol.* 146:393–419

Bozec YM, Alvarez-Filip L, Mumby PJ. 2015. The dynamics of architectural complexity on coral reefs under climate change. *Glob. Change Biol.* 21:223–35

Burke L, Reytar K, Spalding M, Perry A. 2011. *Reefs at risk revisited*. Rep., World Resour. Inst., Washington, DC

Chang S, Elkins C, Alley M, Eaton J, Monismith S. 2009. Flow inside a coral colony measured using magnetic resonance velocimetry. *Limnol. Oceanogr.* 54:1819–27

Chang S, Elkins C, Eaton JK, Monismith S. 2013. Local mass transfer measurements for corals and other complex geometries using gypsum dissolution. *Exp. Fluids* 54:1563

Chang S, Iaccarino G, Ham F, Elkins C, Monismith S. 2014. Local shear and mass transfer on individual coral colonies: computations in unidirectional and wave-driven flows. *J. Geophys. Res. Oceans* 119:2599–619

Chirayath V, Earle SA. 2016. Drones that see through waves-preliminary results from airborne fluid lensing for centimeter-scale aquatic conservation. *Aquat. Conserv. Mar. Freshw. Ecosyst.* 26:237–50

Christoffersen JB, Jonsson IC. 1985. Bed friction and dissipation in a combined current and wave motion. *Ocean Eng.* 12:387–423

Claussen M. 1990. Area-averaging of surface fluxes in a neutrally stratified, horizontally inhomogeneous atmospheric boundary layer. *Atmos. Environ. A* 24:1349–60

Coles D. 1956. The law of the wake in the turbulent boundary layer. *J. Fluid Mech.* 1:191–226

Davis KA, Arthur RS, Reid EC, Rogers JS, Fringer OB, et al. 2020. Fate of internal waves on a shallow shelf. *J. Geophys. Res. Oceans.* 125:e2019JC015377

Davis KA, Leichter JJ, Hench JL, Monismith SG. 2008. Effects of western boundary current dynamics on the internal wave field of the Southeast Florida shelf. *J. Geophys. Res. Oceans* 113:C09010

Davis KA, Monismith SG. 2011. The modification of bottom boundary layer turbulence and mixing by internal waves shoaling on a barrier reef. *J. Phys. Oceanogr.* 41:2223–41

Dawson DA, Trass O. 1972. Mass transfer at rough surfaces. *Int. J. Heat Mass Transf.* 15:1317–36

D'elia CF, Wiebe WJ. 1990. Biogeochemical nutrient cycles in coral-reef ecosystems. *Ecosyst. World* 25:49–74

Dipprey DF, Sabersky RH. 1963. Heat and momentum transfer in smooth and rough tubes at various Prandtl numbers. *Int. J. Heat Mass Transf.* 6:329–53

Dixen M, Hatipoglu F, Sumer BM, Fredsøe J. 2008. Wave boundary layer over a stone-covered bed. *Coast. Eng.* 55:1–20

Duvall MS, Hench JL, Rosman JH. 2019. Collapsing complexity: quantifying multiscale properties of reef topography. *J. Geophys. Res. Oceans* 124:5021–38
Dvorak FA. 1969. Calculation of turbulent boundary layers on rough surfaces in pressure gradients. *AIAA J.* 7:1752–59
Falter JL, Atkinson MJ, Coimbra CF. 2005. Effects of surface roughness and oscillatory flow on the dissolution of plaster forms: evidence for nutrient mass transfer to coral reef communities. *Limnol. Oceanogr.* 50:246–54
Falter JL, Atkinson MJ, Lowe RJ, Monismith SG, Koseff JR. 2007. Effects of nonlocal turbulence on the mass transfer of dissolved species to reef corals. *Limnol. Oceanogr.* 52:274–85
Falter JL, Atkinson MJ, Merrifield M. 2004. Mass-transfer limitation of nutrient uptake by a wave-dominated reef flat community. *Limnol. Oceanogr.* 49:1820–31
Falter JL, Lowe RJ, Atkinson MJ, Cuet P. 2012. Seasonal coupling and de-coupling of net calcification rates from coral reef metabolism and carbonate chemistry at Ningaloo Reef, Western Australia. *J. Geophys. Res. Oceans* 117:C05003
Falter JL, Lowe RJ, Zhang Z. 2016. Toward a universal mass-momentum transfer relationship for predicting nutrient uptake and metabolite exchange in benthic reef communities. *Geophys. Res. Lett.* 43:9764–72
Falter JL, Lowe RJ, Zhang Z, McCulloch M. 2013. Physical and biological controls on the carbonate chemistry of coral reef waters: effects of metabolism, wave forcing, sea level, and geomorphology. *PLOS ONE* 8:e53303
Feddersen F, Guza RT, Elgar S, Herbers THC. 2000. Velocity moments in alongshore bottom stress parameterizations. *J. Geophys. Res. Oceans* 105:8673–86
Ferrari R, McKinnon D, He H, Smith RN, Corke P, et al. 2016. Quantifying multiscale habitat structural complexity: a cost-effective framework for underwater 3D modelling. *Remote Sens.* 8:113
Ferrario F, Beck M, Storlazzi C, Micheli F, Shepard C, Airoldi L. 2014. The effectiveness of coral reefs for coastal hazard risk reduction and adaptation. *Nat. Commun.* 5:3794
Finnigan JJ. 2000. Turbulence in plant canopies. *Annu. Rev. Fluid Mech.* 32:519–71
Finnigan JJ, Shaw RH, Patton EG. 2009. Turbulence structure above a vegetation canopy. *J. Fluid Mech.* 637:387–424
Flack KA, Schultz MP. 2010. Review of hydraulic roughness scales in the fully rough regime. *J. Fluids Eng.* 132:041203
Flack KA, Schultz MP, Shapiro TA. 2005. Experimental support for Townsend's Reynolds number similarity hypothesis on rough walls. *Phys. Fluids* 17:035102
Fredsøe J, Deigaard R. 1992. *Mechanics of Coastal Sediment Transport*. Singapore: World Sci.
Genin A, Monismith SG, Reidenbach MA, Yahel G, Koseff JR. 2009. Intense benthic grazing of phytoplankton in a coral reef. *Limnol. Oceanogr.* 54:938–51
Gerritsen F. 1981. *Wave attenuation and wave set-up on a coastal reef*. Tech. Rep., Univ. Hawaii, Honolulu
Ghisalberti M, Nepf HM. 2002. Mixing layers and coherent structures in vegetated aquatic flows. *J. Geophys. Res. Oceans* 107:3-1–11
Ghisalberti M, Nepf HM. 2006. The structure of the shear layer in flows over rigid and flexible canopies. *Environ. Fluid Mech.* 6:277–301
Goldstein RJ, Karni J. 1984. The effect of a wall boundary-layer on local mass transfer from a cylinder in crossflow. *ASME J. Heat Transf.* 106:260–67
Graham NAJ, Nash KL. 2013. The importance of structural complexity in coral reef ecosystems. *Coral Reefs* 32:315–26
Grant WD, Madsen OS. 1979. Combined wave and current interaction with a rough bottom. *J. Geophys. Res. Oceans* 84:1797–807
Grant WD, Madsen OS. 1986. The continental shelf bottom boundary layer. *Annu. Rev. Fluid Mech.* 18:265–305
Gratwicke B, Speight MR. 2005. Effects of habitat complexity on Caribbean marine fish assemblages. *Mar. Ecol. Prog. Ser.* 292:301–10
Green A. 2002. *Status of coral reefs on the main volcanic islands of American Samoa: a resurvey of long term monitoring sites (benthic communities, fish communities, and key macroinvertebrates)*. Rep., Dep. Mar. Wildl. Resour., Pago Pago, Am. Samoa

Gregg MC, D'Asaro EA, Riley JJ, Kunze E. 2018. Mixing efficiency in the ocean. *Annu. Rev. Mar. Sci.* 10:443–73

Gruber RK, Lowe RJ, Falter JL. 2019. Tidal and seasonal forcing of dissolved nutrient fluxes in reef communities. *Biogeosciences* 16:1921–35

Guo J, Julien PY. 2006. Application of modified log-wake law in open-channels. In *World Environmental and Water Resource Congress 2006: Examining the Confluence of Environmental and Water Concerns*, ed. R Graham. Reston, VA: Am. Soc. Civil Eng. **https://doi.org/10.1061/40856(200)71**

Harborne AR, Mumby PJ, Ferrari R. 2012. The effectiveness of different meso-scale rugosity metrics for predicting intra-habitat variation in coral-reef fish assemblages. *Environ. Biol. Fish* 94:431–42

Hearn CJ. 1999. Wave-breaking hydrodynamics within coral reef systems and the effect of changing relative sea level. *J. Geophys. Res. Oceans* 104:30007–19

Hearn CJ, Atkinson M, Falter J. 2001. A physical derivation of nutrient-uptake rates in coral reefs: effects of roughness and waves. *Coral Reefs* 20:347–56

Heathershaw AD, Simpson JH. 1978. The sampling variability of the Reynolds stress and its relation to boundary shear stress and drag coefficient measurements. *Estuar. Coast. Shelf Sci.* 6:263–74

Hench JL, Rosman JH. 2013. Observations of spatial flow patterns at the coral colony scale on a shallow reef flat. *J. Geophys. Res. Oceans* 118:1142–56

Holbrook SJ, Brooks AJ, Schmitt RJ. 2002. Variation in structural attributes of patch-forming corals and in patterns of abundance of associated fishes. *Mar. Freshw Res.* 53:1045–53

Huang ZC, Lenain L, Melville WK, Middleton JH, Reineman B, et al. 2012. Dissipation of wave energy and turbulence in a shallow coral reef lagoon. *J. Geophys. Res. Oceans* 117:4063–71

Hughes TP, Kerry JT, Álvarez-Noriega M, Álvarez-Romero J, Anderson KD, et al. 2017. Global warming and recurrent mass bleaching of corals. *Nature* 543:373–77

Ivey GN, Winters KB, Koseff JR. 2008. Density stratification, turbulence, but how much mixing? *Annu. Rev. Fluid Mech.* 40:169–84

Jackson PS. 1981. On the displacement height in the logarithmic velocity profile. *J. Fluid Mech.* 1111981:15–25

Jaramillo S, Pawlak G. 2011. AUV-based bed roughness mapping over a tropical reef. *Coral Reefs* 30:11–23

Jiménez J. 2004. Turbulent flows over rough walls. *Annu. Rev. Fluid Mech.* 36:173–96

Jiménez J. 2012. Cascades in wall-bounded turbulence. *Annu. Rev. Fluid Mech.* 44:27–45

Jones NL, Monismith SG. 2008. The influence of whitecapping waves on the vertical structure of turbulence in a shallow estuarine embayment. *J. Phys. Oceanogr.* 38:1563–80

Jonsson IG. 1967. Wave boundary layers and friction factors. In *Coastal Engineering 1966*, pp. 127–48. Reston, VA: Am. Soc. Civil Eng.

Kaimal JC, Wyngaard JC, Izumi Y, Coté OR. 1972. Spectral characteristics of surface layer turbulence. *Q. J. R. Meteorol. Soc.* 98:563–89

Kamphuis JW. 1975. Friction factor under oscillatory waves. *J. Waterw. Harb. Coast. Eng. Div.* 101:135–44

Leichter JJ, Helmuth B, Fischer AM. 2006. Variation beneath the surface: quantifying complex thermal environments on coral reefs in the Caribbean, Bahamas and Florida. *J. Mar. Res.* 64:563–88

Leichter JJ, Wing SR, Miller SL, Denny MW. 1996. Pulsed delivery of subthermocline water to Conch Reef (Florida Keys) by internal tidal bores. *Limnol. Oceanogr.* 41:1490–501

Lentz SJ, Churchill JH, Davis KA. 2018. Coral reef drag coefficients—surface gravity wave enhancement. *J. Phys. Oceanogr.* 48:1555–66

Lentz SJ, Churchill JH, Davis KA, Farrar JT, Pineda J, Starczak V. 2016. The characteristics and dynamics of wave-driven flow across a platform coral reef in the Red Sea. *J. Geophys. Res. Oceans* 121:1360–76

Lentz SJ, Davis KA, Churchill JH, DeCarlo TM. 2017. Coral reef drag coefficients-water depth dependence. *J. Phys. Oceanogr.* 47:1061–75

Leonardi S, Orlandi P, Smalley RJ, Djenidi L, Antonia RA. 2003. Direct numerical simulations of turbulent channel flow with transverse square bars on one wall. *J. Fluid Mech.* 491:229–38

Lesser MP. 1997. Oxidative stress causes coral bleaching during exposure to elevated temperatures. *Coral Reefs* 16:187–92

Long CE, Wiberg PL, Nowell AR. 1993. Evaluation of von Karman's constant from integral flow parameters. *J. Hydraul. Eng.* 119:1182–90

Long MH, Rheuban JE, McCorkle DC, Burdige DJ, Zimmerman RC. 2019. Closing the oxygen mass balance in shallow coastal ecosystems. *Limnol. Oceanogr.* 64:2694–708
Longuet-Higgins MS, Stewart R. 1962. Radiation stress and mass transport in gravity waves with application to 'surf beats.' *J. Fluid Mech.* 13:481–504
Lowe RJ, Falter JL. 2015. Oceanic forcing of coral reefs. *Annu. Rev. Mar. Sci.* 7:43–66
Lowe RJ, Falter JL, Bandet MD, Pawlak G, Atkinson MJ, et al. 2005a. Spectral wave dissipation over a barrier reef. *J. Geophys. Res. Oceans* 110:C04001
Lowe RJ, Falter JL, Koseff JR, Monismith SG, Atkinson MJ. 2007. Spectral wave flow attenuation within submerged canopies: implications for wave energy dissipation. *J. Geophys. Res. Oceans* 112:C05018
Lowe RJ, Koseff JR, Monismith SG. 2005b. Oscillatory flow through submerged canopies: 1. Velocity structure. *J. Geophys. Res. Oceans* 110:C10016
Lowe RJ, Koseff JR, Monismith SG, Falter JL. 2005c. Oscillatory flow through submerged canopies: 2. Canopy mass transfer. *J. Geophys. Res. Oceans* 110:C10017
Lowe RJ, Shavit U, Falter JL, Koseff JR, Monismith SG. 2008. Modeling flow in coral communities with and without waves: a synthesis of porous media and canopy flow approaches. *Limnol. Oceanogr.* 53:2668–80
Lueck RG, Lu Y. 1997. The logarithmic layer in a tidal channel. *Cont. Shelf Res.* 17:1785–801
Lugo-Fernandez A, Roberts HH, Wiseman WJ, Carter BL. 1998. Water level and currents of tidal and infragravity periods at Tague Reef, St. Croix (USVI). *Coral Reefs* 17:343–49
Luhar M, Rominger J, Nepf H. 2008. Interaction between flow, transport, and vegetation spatial structure. *Environ. Fluid. Mech.* 8:423–39
Madsen OS. 1994. Spectral wave-current bottom boundary layer flows. In *Coastal Engineering 1994*, ed. BL Edge, pp. 623–34. Reston, VA: Am. Soc. Civ. Eng.
Mahrt L. 1987. Grid-averaged surface fluxes. *Mon. Weath. Rev.* 115:1550–60
Mahrt L. 2000. Surface heterogeneity and vertical structure of the boundary layer. *Bound. Layer Meteorol.* 96:33–62
Mason PJ. 1988. The formation of areally averaged roughness lengths. *Q. J. R. Meteorol. Soc.* 114:399–420
McClanahan TR, Maina J, Moothien-Pillay R, Baker AC. 2005. Effects of geography, taxa, water flow, and temperature variation on coral bleaching intensity in Mauritius. *Mar. Ecol. Prog. Ser.* 71:130–34
McDonald CB, Koseff JR, Monismith SG. 2006. Effects of the depth to coral height ratio on drag coefficients for unidirectional flow over coral. *Limnol. Oceanogr.* 51:1294–301
Molina L, Pawlak G, Wells JR, Monismith SG, Merrifield MA. 2014. Diurnal cross-shore thermal exchange on a tropical forereef. *J. Geophys. Res. Oceans* 119:6101–20
Moltchanov S, Bohbot-Raviv Y, Duman T, Shavit U. 2015. Canopy edge flow: a momentum balance analysis. *Water Resour. Res.* 51:2081–95
Monismith SG. 2007. Hydrodynamics of coral reefs. *Annu. Rev. Fluid Mech.* 39:37–55
Monismith SG, Davis KA, Shellenbarger GG, Hench JL, Nidzieko NJ, et al. 2010. Flow effects on benthic grazing on phytoplankton by a Caribbean reef. *Limnol. Oceanogr.* 55:1881–92
Monismith SG, Genin A, Reidenbach MA, Yahel G, Koseff JR. 2006. Thermally driven exchanges between a coral reef and the adjoining ocean. *J. Phys. Oceanogr.* 36:1332–47
Monismith SG, Herdman LM, Ahmerkamp S, Hench JL. 2013. Wave transformation and wave-driven flow across a steep coral reef. *J. Phys. Oceanogr.* 43:1356–79
Monismith SG, Koseff JR, White BL. 2018. Mixing efficiency in the presence of stratification: Is it constant? *Geophys. Res. Lett.* 45:5627–34
Monismith SG, Rogers JS, Koweek D, Dunbar RB. 2015. Frictional wave dissipation on a remarkably rough reef. *Geophys. Res. Lett.* 42:4063–71
Nakamura T, van Woesik R. 2001. Water-flow rates and passive diffusion partially explain differential survival of corals during the 1998 bleaching event. *Mar. Ecol. Prog. Ser.* 212:301–4
Nakamura T, van Woesik R, Yamasaki H. 2005. Photoinhibition of photosynthesis is reduced by water flow in the reef-building coral *Acropora digitifera*. *Mar. Ecol. Prog. Ser.* 301:109–18
Napoli E, Armenio V, DeMarchis M. 2008. The effect of the slope of irregularly distributed roughness elements on turbulent wall-bounded flows. *J. Fluid Mech.* 613:385–94
Nelson RC. 1996. Hydraulic roughness of coral reef platforms. *Appl. Ocean Res.* 18:265–74

Nepf HM. 2012. Flow and transport in regions with aquatic vegetation. *Annu. Rev. Fluid Mech.* 44:123–42
Nepf HM, Vivoni ER. 2000. Flow structure in depth-limited, vegetated flow. *J. Geophys. Res. Oceans* 105:28547–57
Nezu I, Nakagawa H. 1993. *Turbulence in Open-Channel Flows*. Rotterdam, Neth.: Balkema
Nielsen P. 1992. *Coastal Bottom Boundary Layers and Sediment Transport*. Singapore: World Sci.
Nikuradse J. 1933. *Stromungsgesetze in rauhen Robren*. Düsseldorf, Ger.: Ver. Dtsch. Ing.
Nunes V, Pawlak G. 2008. Observations of bed roughness of a coral reef. *J. Coast. Res.* 24(SP2):39–50
Pan Y, Banerjee S. 1995. A numerical study of free-surface turbulence in channel flow. *Phys. Fluids* 7:1649–64
Pawlak G, MacCready P. 2002. Oscillatory flow across an irregular boundary. *J. Geophys. Res. Oceans* 107:4-1–17
Péquignet A-C, Becker JM, Merrifield MA, Boc SJ. 2011. The dissipation of wind wave energy across a fringing reef at Ipan. *Coral Reefs* 30:71–82
Perry AE, Schofield WH, Joubert PN. 1969. Rough wall turbulent boundary layers. *J. Fluid Mech.* 37:383–413
Pomeroy AW, Lowe RJ, Symonds G, Van Dongeren AR, Moore C. 2012. The dynamics of infragravity wave transformation over a fringing reef. *J. Geophys. Res. Oceans* 117:C11022
Pomeroy AW, Lowe RJ, Van Dongeren AR, Ghisalberti M, Bodde W, Roelvink D. 2015. Spectral wave-driven sediment transport across a fringing reef. *Coast. Eng.* 98:78–94
Pope SB. 2000. *Turbulent Flows*. Cambridge, UK: Cambridge Univ. Press
Rajagopalan K. 2010. *Large eddy simulation of turbulent boundary layers over rough bathymetry*. PhD Thesis, Univ. Hawaii, Honolulu
Raupach MR. 1992. Drag and drag partition on rough surfaces. *Bound. Layer Meteorol.* 60:375–95
Raupach MR, Antonia RA, Rajagopalan S. 1991. Rough-wall turbulent boundary layers. *Appl. Mech. Rev.* 44:1–25
Raupach MR, Finnigan JJ, Brunet Y. 1996. Coherent eddies and turbulence in vegetation canopies: the mixing-layer analogy. In *Boundary-Layer Meteorology: 25th Anniversary Volume, 1970–1995*, ed. JR Garratt, PA Taylor, pp. 351–82. Dordrecht, Neth.: Springer
Raupach MR, Shaw R. 1982. Averaging procedures for flow within vegetation canopies. *Bound. Layer Meteorol.* 22:79–90
Raupach MR, Thom AS. 1981. Turbulence in and above plant canopies. *Annu. Rev. Fluid Mech.* 13:97–129
Reid EC, DeCarlo TM, Cohen AL, Wong GT, Lentz SJ, et al. 2019. Internal waves influence the thermal and nutrient environment on a shallow coral reef. *Limnol. Oceanogr.* 64:1949–65
Reidenbach MA, Koseff JR, Koehl MAR. 2009. Hydrodynamic forces on larvae affect their settlement on coral reefs in turbulent, wave-driven flow. *Limnol. Oceanogr.* 54:318–30
Reidenbach MA, Koseff JR, Monismith SG. 2007. Laboratory experiments of fine-scale mixing and mass transport within a coral canopy. *Phys. Fluids* 19:075107
Reidenbach MA, Monismith SG, Koseff JR, Yahel G, Genin A. 2006. Boundary layer turbulence and flow structure over a fringing coral reef. *Limnol. Oceanogr.* 51:1956–68
Ribes M, Atkinson MJ. 2007. Effects of water velocity on picoplankton uptake by coral reef communities. *Coral Reefs* 26:413–21
Risk MJ. 1972. Fish diversity on a coral reef in the Virgin Islands. *Atoll Res. Bull.* 153:1–4
Rogers JS, Maticka SA, Chirayath V, Woodson CB, Alonso JJ, Monismith SG. 2018. Connecting flow over complex terrain to hydrodynamic roughness on a coral reef. *J. Phys. Oceanogr.* 48:1567–87
Rogers JS, Monismith SG, Dunbar RB, Koweek D. 2015. Field observations of wave-driven circulation over spur and groove formations on a coral reef. *J. Geophys. Res. Oceans* 120:145–60
Rominger JT, Nepf HM. 2011. Flow adjustment and interior flow associated with a rectangular porous obstruction. *J. Fluid Mech.* 680:636–59
Rosman JH, Hench JL. 2011. A framework for understanding drag parameterizations for coral reefs. *J. Geophys. Res. Oceans* 116:C08025
Sanford TB, Lien RC. 1999. Turbulent properties in a homogeneous tidal bottom boundary layer. *J. Geophys. Res. Oceans* 104:1245–57
Sanitjai S, Goldstein RJ. 2004. Heat transfer from a circular cylinder to mixtures of water and ethylene glycol. *Int. J. Heat Mass Transf.* 47:4785–94
Sarpkaya T. 1975. Forces on cylinders and spheres in a sinusoidally oscillating fluid. *J. Appl. Mech. Mar.* 42:32–37

Schlichting H. 1937. *Experimental investigation of the problem of surface roughness*. Tech. Memo. 823, Natl. Advis. Comm. Aeronaut., Washington, DC
Schultz MP, Flack KA. 2009. Turbulent boundary layers on a systematically-varied rough wall. *Phys. Fluids* 21:015104
Sebens KP, Grace SP, Helmuth B, Maney EJ, Miles JS. 1998. Water flow and prey capture by three scleractinian corals, *Madracis mirabilis*, *Montastrea cavernosa* and *Porites porites*, in a field enclosure. *Mar. Biol.* 131:347–60
Sebens KP, Helmuth B, Carrington E, Agius B. 2003. Effects of water flow on growth and energetics of the scleractinian coral *Agaricia tenuifolia* in Belize. *Coral Reefs* 22:35–47
Sebens KP, Witting J, Helmuth BST. 1997. Effects of water flow and branch spacing on particle capture by the reef coral *Madracis mirabilis* (Duchassaing and Michelotti). *J. Exp. Mar. Biol. Ecol.* 211:1–28
Shapiro OH, Fernandez VI, Garren M, Guasto JS, Debaillon-Vesque FP, et al. 2014. Vortical ciliary flows actively enhance mass transport in reef corals. *PNAS* 111:13391–96
Shih LH, Koseff JR, Ivey GN, Ferziger JH. 2005. Parameterization of turbulent fluxes and scales using homogeneous sheared stably stratified turbulence simulations. *J. Fluid Mech.* 525:193–214
Sigal A, Danberg JE. 1990. New correlation of roughness density effect on the turbulent boundary layer. *AIAA J.* 28:554–56
Sleath JFA. 1987. Turbulent oscillatory flow over rough beds. *J. Fluid Mech.* 182:369–409
Stacey MT, Monismith SG, Burau JR. 1999. Measurements of Reynolds stress profiles in unstratified tidal flow. *J. Geophys. Res. Oceans* 104:10933–49
Stocking JB, Laforsch C, Sigl R, Reidenbach MA. 2018. The role of turbulent hydrodynamics and surface morphology on heat and mass transfer in corals. *J. R. Soc. Interface* 15:20180448
Stocking JB, Rippe JP, Reidenbach MA. 2016. Structure and dynamics of turbulent boundary layer flow over healthy and algae-covered corals. *Coral Reefs* 35:1047–59
Storlazzi C, Logan J, Field M. 2003. Quantitative morphology of a fringing reef tract from high-resolution laser bathymetry: southern Molokai, Hawaii. *Geol. Soc. Am. Bull.* 115:1344–55
Swart D. 1974. *Offshore sediment transport and equilibrium beach profiles*. Tech. Rep. 131, Delft Hydraul. Lab., Delft, Neth.
Taebi S, Lowe RJ, Pattiaratchi CB, Ivey GN, Symonds G, Brinkman R. 2011. Nearshore circulation in a tropical fringing reef system. *J. Geophys. Res. Oceans* 116:C02016
Takeshita Y, McGillis W, Briggs EM, Carter AL, Donham EM, et al. 2016. Assessment of net community production and calcification of a coral reef using a boundary layer approach. *J. Geophys. Res. Oceans* 121:5655–71
Talke SA, Horner-Devine AR, Chickadel CC, Jessup AT. 2013. Turbulent kinetic energy and coherent structures in a tidal river. *J. Geophys. Res. Oceans* 118:6965–81
Tanino Y, Nepf HM. 2008. Laboratory investigation of mean drag in a random array of rigid, emergent cylinders. *J. Hydraul. Eng.* 134:34–41
Taylor PA. 1987. Comments and further analysis on effective roughness lengths for use in numerical three-dimensional models. *Bound. Layer Meteorol.* 39:403–18
Teixeira MAC, Belcher SE. 2002. On the distribution of turbulence by a progressive surface wave. *J. Fluid Mech.* 458:229–67
Teneva L, Dunbar RB, Mucciarone DA, Dunckley JF, Koseff JR. 2013. High-resolution carbon budgets on a Palau back-reef modulated by interactions between hydrodynamics and reef metabolism. *Limnol. Oceanogr.* 58:1851–70
Terray EA, Donelan MA, Agrawal YC, Drennan WM, Kahma KK, et al. 1996. Estimates of kinetic energy dissipation under breaking waves. *J. Phys. Oceanogr.* 26:792–807
Thomas FIM, Atkinson MJ. 1997. Ammonium uptake by coral reefs: effects of water velocity and surface roughness on mass transfer. *Limnol. Oceanogr.* 42:81–88
Trowbridge JH, Lentz SJ. 2018. The bottom boundary layer. *Annu. Rev. Mar. Sci.* 10:397–420
Turner JS. 1973. *Buoyancy Effects in Fluids*. Cambridge, UK: Cambridge Univ. Press
van Rij JA, Belnap BJ, Ligrani PM. 2002. Analysis and experiments on three-dimensional, irregular surface roughness. *J. Fluids Eng.* 124:671–77

van Woesik R, Irikawa A, Anzai R, Nakamura T. 2012. Effects of coral colony morphologies on mass transfer and susceptibility to thermal stress. *Coral Reefs*. 31:633–39

Veron JEN. 1995. *Corals in Space and Time: The Biogeography and Evolution of the Scleractinia*. Ithaca, NY: Cornell Univ. Press

Walter RK, Nidzieko NJ, Monismith SG. 2011. Similarity scaling of turbulence spectra and cospectra in a shallow tidal flow. *J. Geophys. Res. Oceans* 116:C10019

Warner SJ, MacCready P. 2009. Dissecting the pressure field in tidal flow past a headland: When is form drag "real"? *J. Phys. Oceanogr.* 39:2971–84

Wolanski E, Delesalle B. 1995. Upwelling by internal waves, Tahiti, French Polynesia. *Cont. Shelf Res.* 15:357–68

Wooding RA, Bradley EF, Marshall JK. 1973. Drag due to regular arrays of roughness elements of varying geometry. *Bound. Layer Meteorol.* 5:285–308

Wright DG, Thompson KR. 1983. Time-averaged forms of the nonlinear stress law. *J. Phys. Oceanogr.* 13:341–45

Wyatt AS, Falter JL, Lowe RJ, Humphries S, Waite AM. 2012. Oceanographic forcing of nutrient uptake and release over a fringing coral reef. *Limnol. Oceanogr.* 57:401–19

Yaglom AM, Kader BA. 1974. Heat and mass transfer between a rough wall and turbulent fluid flow at high Reynolds and Péclet numbers. *J. Fluid Mech.* 62:601–23

Yates KK, Zawada DG, Smiley NA, Tiling-Range G. 2017. Divergence of seafloor elevation and sea level rise in coral reef ecosystems. *Biogeosciences* 14:1739

Yu X, Rosman JH, Hench JL. 2018. Interaction of waves with idealized high-relief bottom roughness. *J. Geophys. Res. Oceans* 123:3038–59

Zawada DG, Brock JC. 2009. A multiscale analysis of coral reef topographic complexity using lidar-derived bathymetry. *J. Coast. Res.* 25(SP53):6–15

Annual Review of Marine Science

Volume 13, 2021

Contents

Errata

An online log of corrections to *Annual Review of Marine Science* articles may be found at http://www.annualreviews.org/errata/marine